Acoustic Emission Monitoring of Damage Progression in Fiber Reinforced Polymer Rods

by

Mohammadhadi Shateri

A Thesis submitted to the Faculty of Graduate Studies of The University of Manitoba in partial fulfilment of the requirements of the degree of

MASTER OF SCIENCE

Department of Electrical and Computer Engineering

University of Manitoba

Winnipeg

ABSTRACT

The fiber reinforced polymer (FRP) bars have been widely used in pre-stressing applications and reinforcing of the civil structures. High strength-to-weight ratio and high resistance to the corrosion make the FRP bars a good replacement for steel reinforcing bars in civil engineering applications. According to the CAN/CSA-S806-12 standard, the maximum recommended stress in FRP bars under service loads should not exceed 25% and 65% of the ultimate strength for glass FRP (GFRP) and carbon FRP (CFRP), respectively. These stress values are set to prevent creep failure in FRP bars. However, for in-service applications, there are few physical indicators that these values have been reached or exceeded. In this work analysis of acoustic emission (AE) signals is used. Two new techniques based on pattern recognition and frequency entropy of the isolated acoustic emission (AE) signal are presented for monitoring damage progression and prediction of failure in FRPs.

ACKNOWLEDGEMENT

I would like to thank my supervisor Professor Dr. Douglas Thomson for his support, advice, guidance and encouragement throughout my study.

I gratefully acknowledge the Natural Sciences and Engineering Research Council of Canada, the Government of Manitoba, Research Manitoba and Centre for Structural Innovation and Monitoring Technologies (SIMTReC).

I wish to acknowledge Professor Dr. Dagmar Svecova head of department of Civil engineering and Director of Centre for Structural Innovation and Monitoring Technologies (SIMTReC), and my lab member Maha Ghaib.

Finally thanks to my parents, my family members and my friend Shabnam for their constant support and encouragement.

This thesis is dedicated to my father Hossein and my mother Zahra

For their endless love, support, and encouragement

Table of Contents

LIST OF TABLES

LIST OF FIGURES

CHAPTER 1: INTRODUCTION

Fiber reinforced polymer (FRP) rods have several properties including high strength to weight ratio and excellent corrosion resistance, which make them to be used in different civil engineering installations [1]. The corrosion of the steel reinforcing rods has been known as one of the main reason for shortening the service life of reinforced concrete structures [2]. Therefore, the FRP rods have been introduced to replace the steel reinforcing bars in civil structures.

The FRP rods are a combination of fibers embedded in resin matrix (polymer) which keeps the fibers together. The fibers are the main load-bearing components in FRP rods. Compare to the steel, the resin matrix is very resistant to the corrosion but has lower mechanical capacity. On the other hand the fibers exhibit high strength and stiffness. The idea of fiber reinforced polymer is based on the combining the advantages of the resin matrix and fibers. There are different ways for manufacturing the FRP rods [3]. However, they are mostly produced using pultrusion process (see fig. 1.1).

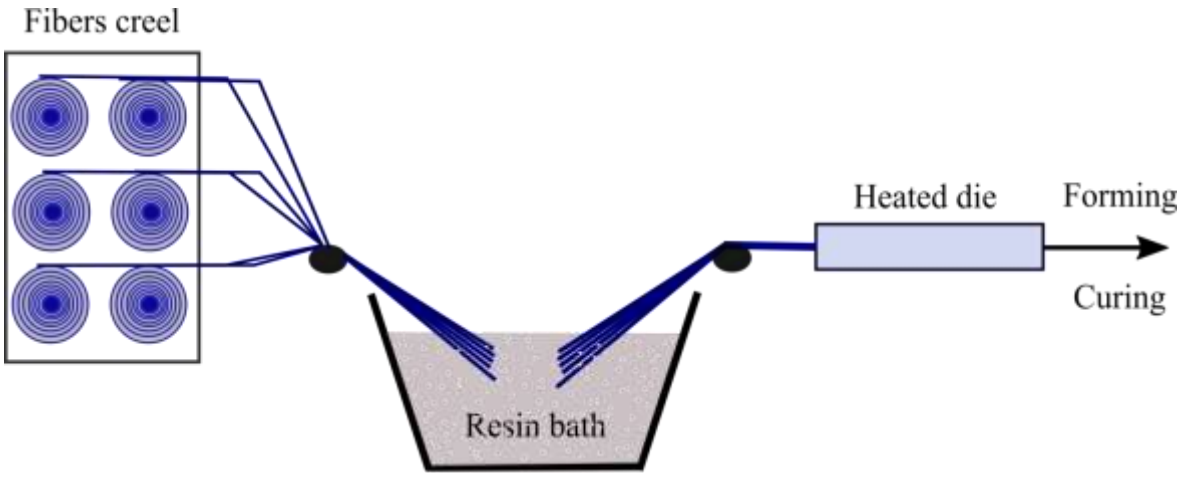

Figure 1. 1 Schematic of pultrusion process for manufacturing of fiber reinforced polymer rods

For the specimens used in this study, fiber is dominating with a volume fraction of 60% to 70%. Two most widely used FRP rods including glass fiber reinforced polymer (GFRP) and carbon fiber reinforced polymer (CFRP) are used. Fig. 1.2 shows an example of the specimens used in this work.

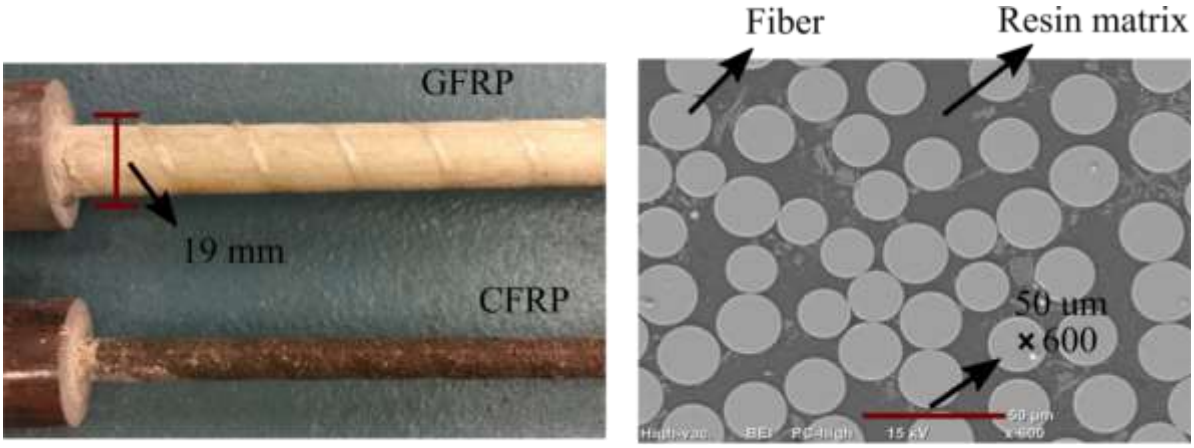

Figure 1. 2 Morphology of the fiber reinforced polymer rods used in this study (a) GFRP and CFRP rods (b) Cross sectional scanning electron microscopic (SEM) image of the FRP rod

Table 1.1 lists the general properties of the tested specimens that is provided by Hughes Brothers Inc. and are manufactured to meet the Canadian standard association (CSA) design and construction of building component with FRP (S806-12). Based on a research study in [4] up to 2012 a total of 190 installations in Canada including bridge decks, parapets, barriers, sidewalks and more than 50 bridge decks in the U.S. have used FRP rods as reinforcement. A study conducted by the ISIS Canada [5] listed some of those bridges in Canada that the FRPs are used in them. For example in the Taylor bridge in Headingley, Manitoba the CFRPs were used for reinforcing the girders and the side walls were reinforced with GFRPs in 1998. ISIS Canada studies reported a durability performance of five to eight

years for the GFRP bars of the in service bridge decks [6]. However, the FRP rods can become damaged due to excessive loading or accidental sources of damage.

Table 1. 1 List of Aslan FRP specimens

	Units	CFRP size2	CFRP size4	GFRP size4	GFRP size6
Guaranteed Tensile Strength	MPa	2241	2068	758	690
Tensile Modulus of Elasticity	GPa	124	124	46	46
Nominal Cross Sectional Area	mm^2	31.67	126.7	126.7	285
Nominal Diameter	mm	6	13	13	19
Ultimate Strain	%	1.81	1.67	1.64	1.49
Surface Coating	-	*	*	**	**

*Sand coated ** Undulation and sand coated

Depending on the geometry, size, morphology and loading condition different damage mechanisms can be generated in the FRP rods. Three main damage mechanisms in FRP rods can be listed as fiber breakage, matrix cracking and fiber-matrix debonding. Fig. 1.3 represents each type of damage mechanism.

Damages in FRPs can degrade the service life of the FRP rods and lead to sudden brittle failure. It is a matter of great importance to develop a technique to provide warning for the impending failure. For the steel reinforcing rods the stress-strain behavior can be used. Fig. 1.4 represents the stress-strain characteristics of various types of FRP rods used in this study in comparison with steel bar. As can be seen from Fig.1 for the steel reinforcing rods the stress-strain in linear up to a point and then it is flat up the failure. This ductile behaviour of steel is used to the advantage of design engineers. Steel reinforced concrete members are usually designed as under-

reinforced, and will demonstrate rapidly increasing deformation after yielding of steel and before failure. On the other hand, the FRP bars lack ductile stress-strain behavior and hence do not provide any prior warning for FRP reinforced concrete structures before impending failure. Therefore, it is important to provide a method that is able to suggest a maximum level of stress/load for in-service application of FRP bars and provide warning before impending failure. According to the CAN/CSA-S806-12 the maximum stress for preventing creep failure in FRP bars under loads at serviceability limit state should not exceed 25% and 65% of the ultimate strength for GFRP and CFRP, respectively.

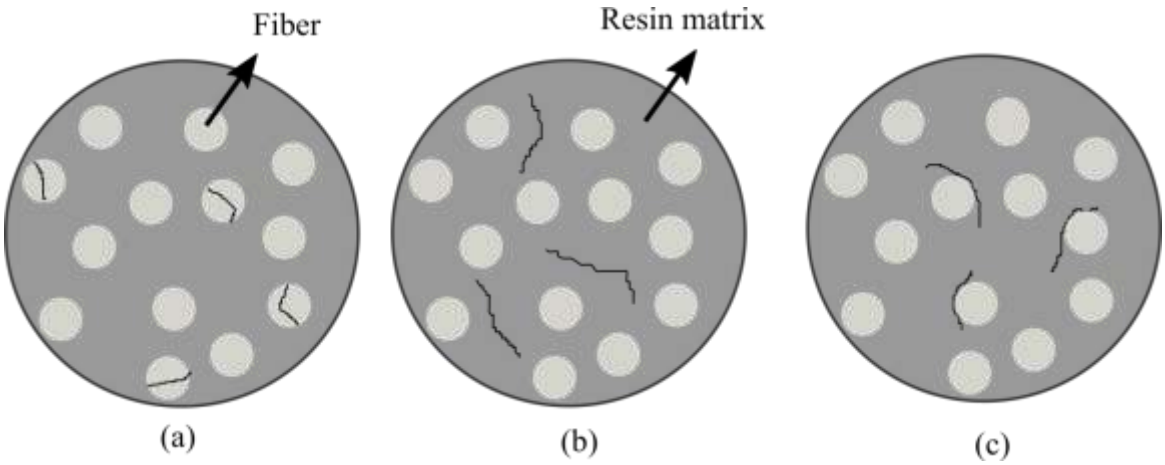

Figure 1. 3 Basic damage mechanisms in fiber reinforced polymer rods (a) Fiber breakage (b) Matrix cracking (c) Fiber-Matrix debonding

Similar statement is used in CAN/CSA S6-14 for the maximum permissible stresses in FRP tendons for pretensioning and post-tensioning systems. Moreover, the American standard ACI440.1R recommends only 20% and 55% as maximum recommended stress on GFRP and CFRP, respectively. For in-service applications there are no physical indicators that these values have been reached or exceed, unless the strain in the bars is being monitored. Furthermore there is no consensus what these values need to be for new generation of FRP bars currently manufactured with much higher strength at failure compared to bars that were available when the code provisions were written.

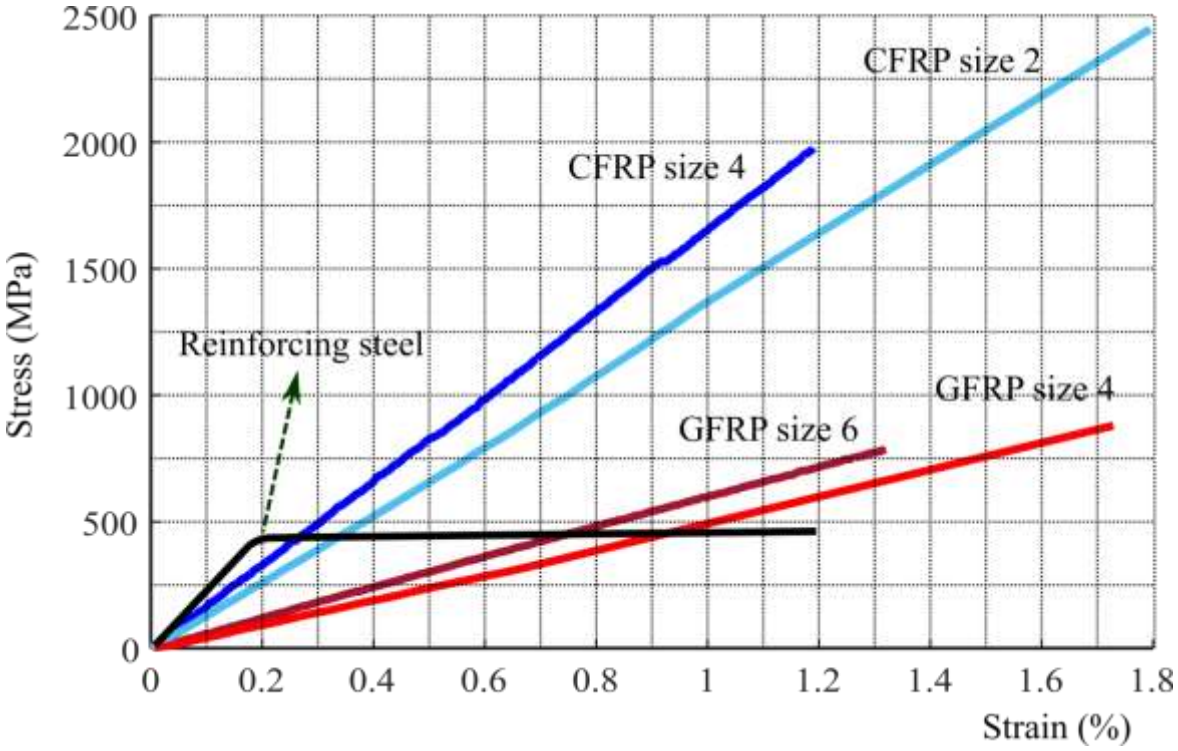

Figure 1. 4 Stress-Strain characteristics of various types of fiber reinforced polymer rods

Studies have revealed that acoustic emission (AE) signal analysis is a promising non-destructive damage monitoring technique for FRP materials [8]. When damage such as fibre breakage, matrix cracking and fiber-matrix debonding occurs in FRP rods there is often a sudden release of mechanical energy that results in acoustic emission signals [7-9]. Fig.1.5 represents histogram of the AE events during tensile loading of FRP rods. These acoustic emission signals are sensed through the AE sensors mounted on the surface of the FRPs and can be analyzed for FRP health monitoring. A large number of studies have been done on composite materials, where AE signal analysing is used for the detection and monitoring of damage. AE signals have characteristics that can be analyzed for damage detection and monitoring of failure modes [7]. Some studies have used time based features extracted from AE event such as peak amplitude, Duration, number of counts and so on (see fig. 1.5) to characterize different damage mechanisms in FRP materials [8-13]. Tsamtsakis et al. [10]

studied the cumulative number of counts collected from tensile test on quasi-isotropic carbon fiber reinforced epoxy laminates to monitor the progression of fatigue damage. Barre´ and Benzeggagh [8] employed the peak amplitude distribution combined with scanning electron microscope (SEM) images to characterize damage mechanisms in glass fiber-reinforced polypropylene.

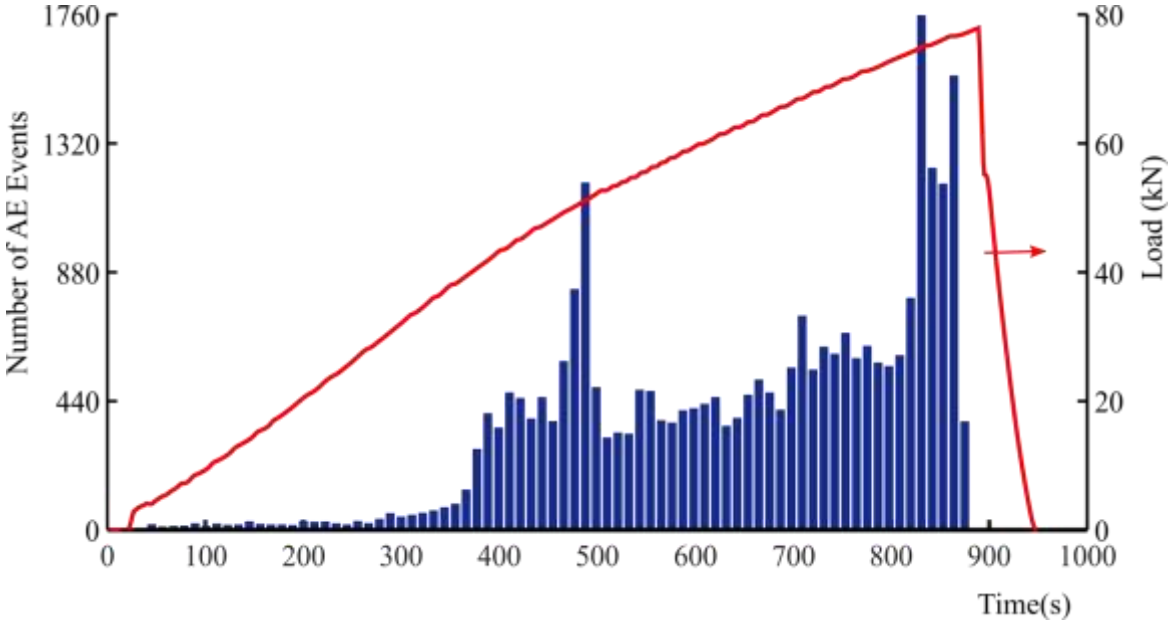

Figure 1. 5 Histogram of acoustic emission events during tensile loading of FRP rod

They concluded that the AE amplitude from 40-55 dB correspond to the matrix cracking, 60-65 dB to interface fracture or debonding, 65-85 dB to fiber pull-out and 85-95 dB to fiber breakage[1]. Komai et al. [13] investigated damage mechanisms in unidirectionally reinforced carbon fiber/epoxy composite using AE time-based features including peak amplitude, duration, number of counts and count/duration combined with SEM images and scanning acoustic microscope (SAM). Some other studies have used pattern recognition algorithms either supervised or unsupervised [14] based on AE time features to characterize damage mechanisms in composite materials. These studies aimed to group the AE signals with

[1] In [8] 0 dB corresponds to 1μV at the transducer.

similar features into clusters and then used clusters to differentiate between damage states [15].

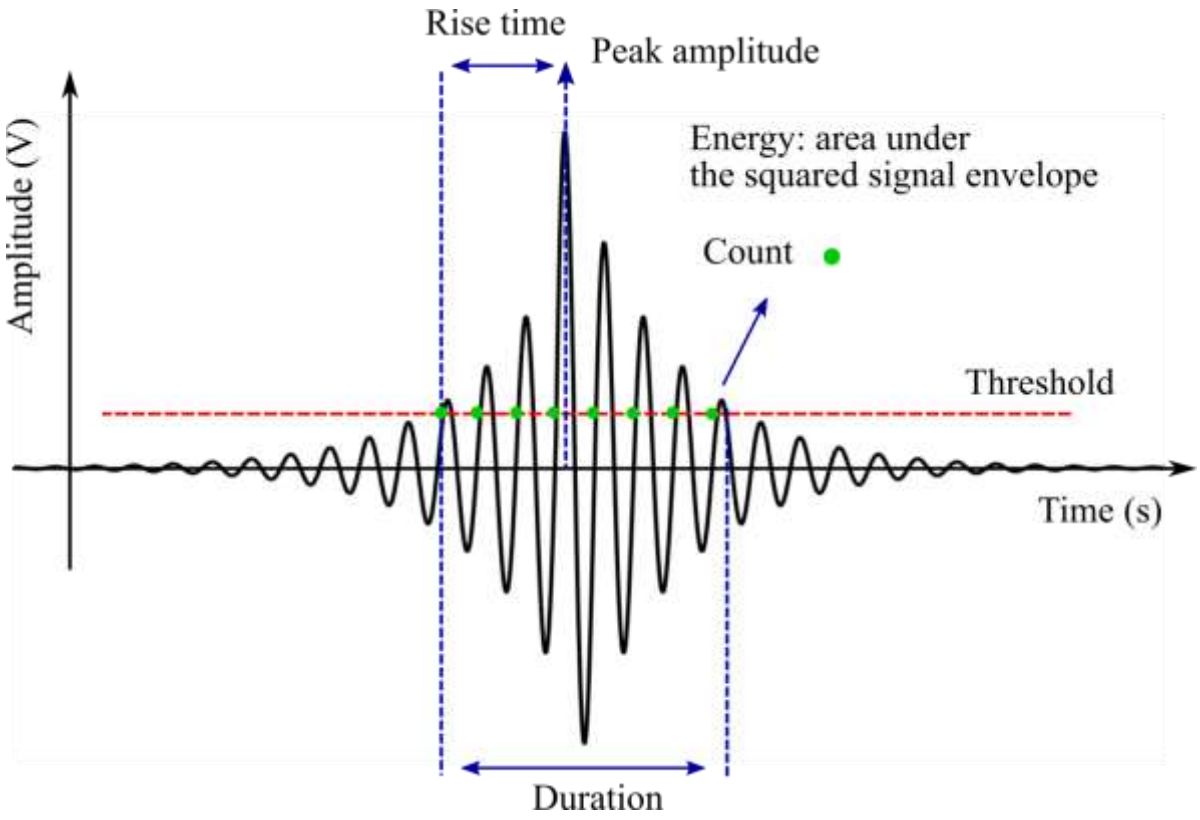

Figure 1. 6 Common time-based features of acoustic emission signal

Studies have used different pattern recognition algorithms to discriminate the AE signals. Marec et al. [16] used fuzzy c-means clustering algorithm coupled with principle component analysis (PCA) to discriminate AE signals in cross-ply composites and SMC. Gutkin et al. [14] used three different pattern recognition techniques including k-means, Self-Organizing Map (SOM) combined with k-means and Competitive Neural network (CNN) for investigating failure in unidirectional carbon/epoxy pre-preg. However, Ni et al. [17] showed that the sensors location can have a dramatic effect on the amplitude attenuation and hence the time descriptors of AE events can be changed while the normalized frequency spectrum is unchanged. They concluded that fast Fourier transform (FFT) and time-frequency method

of wavelet transform (WT) are promising signal analysis tools for investigation of microfailure modes and microfracture mechanisms in composite materials. Characterization of damage mechanisms in composite materials based on the frequency of AE signals were done in [14, 18-20]. It was assumed that different damage mechanisms generate specific frequency range. Fig. 1.7 shows the frequency ranges defined by these studies corresponding to different damage mechanisms in composite materials (See Appendix C).

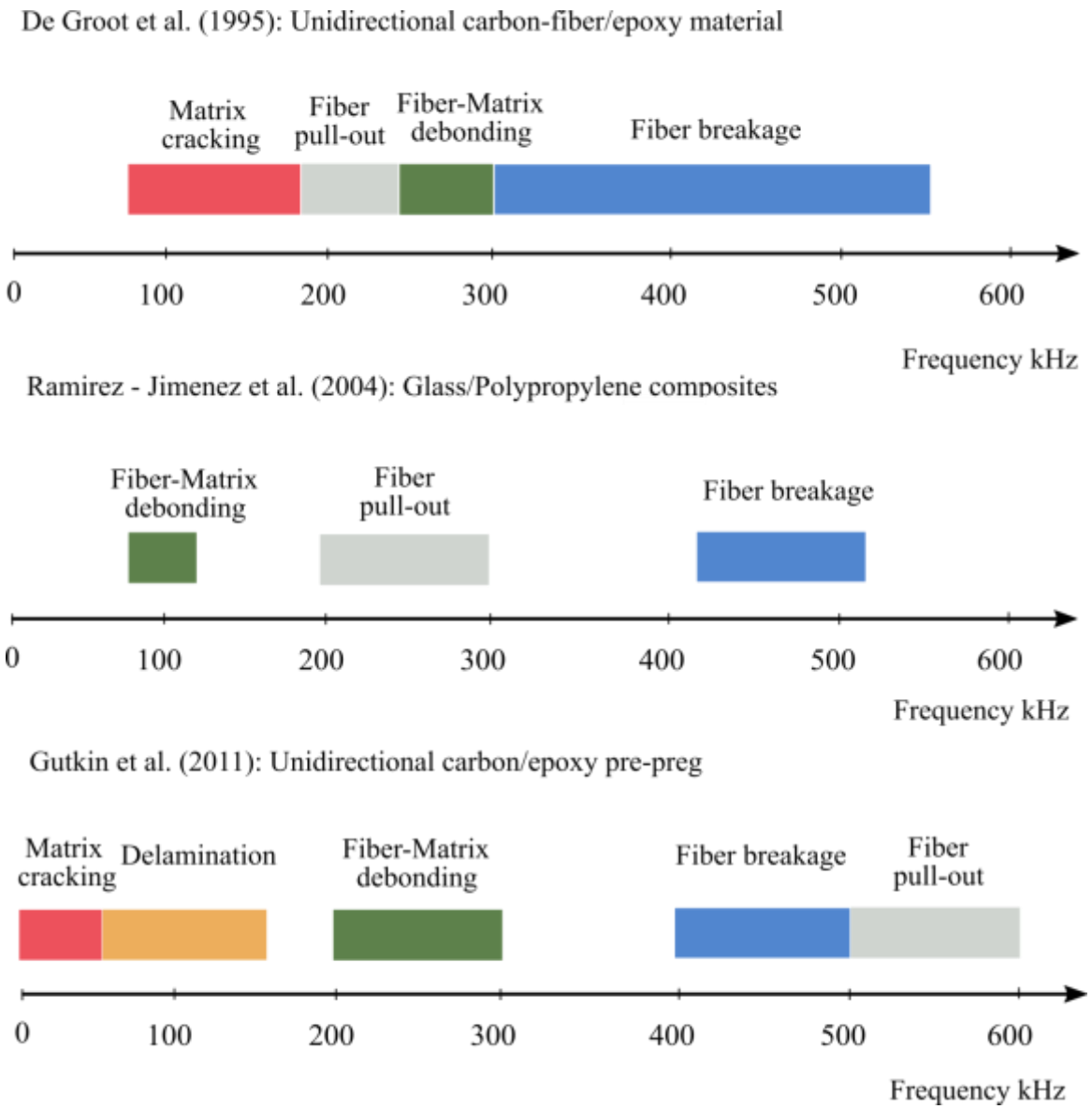

Figure 1.7 Damage characterization based on the peak frequency of AE signals by De Groot et al. [18], Ramirez-Jimenez et al. [19] and Gutkin et al. [14]

In a study by De Groot et al. [18] damage mechanisms in unidirectional carbon-fiber/epoxy material were characterized using the frequency content of acoustic emission signals. They designed specimens that were failed under specific failure modes and then by comparing the peak frequency ranges of those failure modes, different damages were characterized. In some studies [21-22] based on the fact that WT provides better frequency resolution compare to the FT, the WT was used to discriminate the AE events.

Using the WT each AE event was decomposed into different frequency levels and the energy of each level was used for identification of damage mechanisms. Even though there have been many studies for identification of damage mechanisms in FRP materials, none of them have explored a methodology to predict failure in FRP rods. In a study conducted by Unnthorsson et al. [23] the randomness of AE events investigated using entropy was used for prediction of the early failure in FRP materials. In that study four different entropies were defined in time and in frequency. Their results showed that the evolution of average entropy is almost unchanged from 20% to 95% of the FRP's lifetime. Therefore, they concluded that the average entropy cannot be used for early failure prediction.

Failure prediction is important for FRP rods as they are extensively used in pre-stressing applications and have been used for reinforcing in bridge decks [24]. Within the scope of this project and in collaboration with the Centre for Structural Innovation and Monitoring Technologies (SIMTReC) at university of Manitoba, the failure in CFRP and GFRP rods was investigated under the ramping tensile load. Chapter 2 provides information about the experimental procedure and shows how the generated acoustic emission signals using the pencil-lead break test are used to calculate the FRP rods parameters including attenuation coefficient. In chapter 3 a novel AE event detection algorithm, utilizing the RMS envelope, is developed. This method is applied to the AE data to detect each AE event separately, even

when AE events are nearly coincident. A fuzzy c-means (FCM) clustering algorithm is used to classify these detected AE events into clusters. These FCM clusters are used for failure prediction. In chapter 4 AE entropy defined in the frequency domain using Fourier transform (FT) and wavelet transform (WT) of each detected AE events is used as a measure of randomness of AE signals. A new procedure based on the frequency entropy combined with the one-sided Chebyshev's inequality is used to provide warning for the incoming failure in FRP rods.

CHAPTER 2: EXPERIMENTAL PROCEDURE

2.1 Test specimens and instrumentation

The specimens used in this project were from two different types of FRP materials, glass FRP (GFRP) and carbon FRP (CFRP) rods. For the anchoring of the specimens for the tensile test, FRP rods were prepared according to the Canadian standard association (CSA) design and construction of building component with FRP (S806-12). The rods were manufactured to the appropriate length. The properties of the specimens were listed in table 1.1. Expansive grout was employed for anchoring the specimens into the steel pipes. The Instron 300DX and 30kip Baldwin universal testing machines were used for loading the specimens (see fig. 2.1).

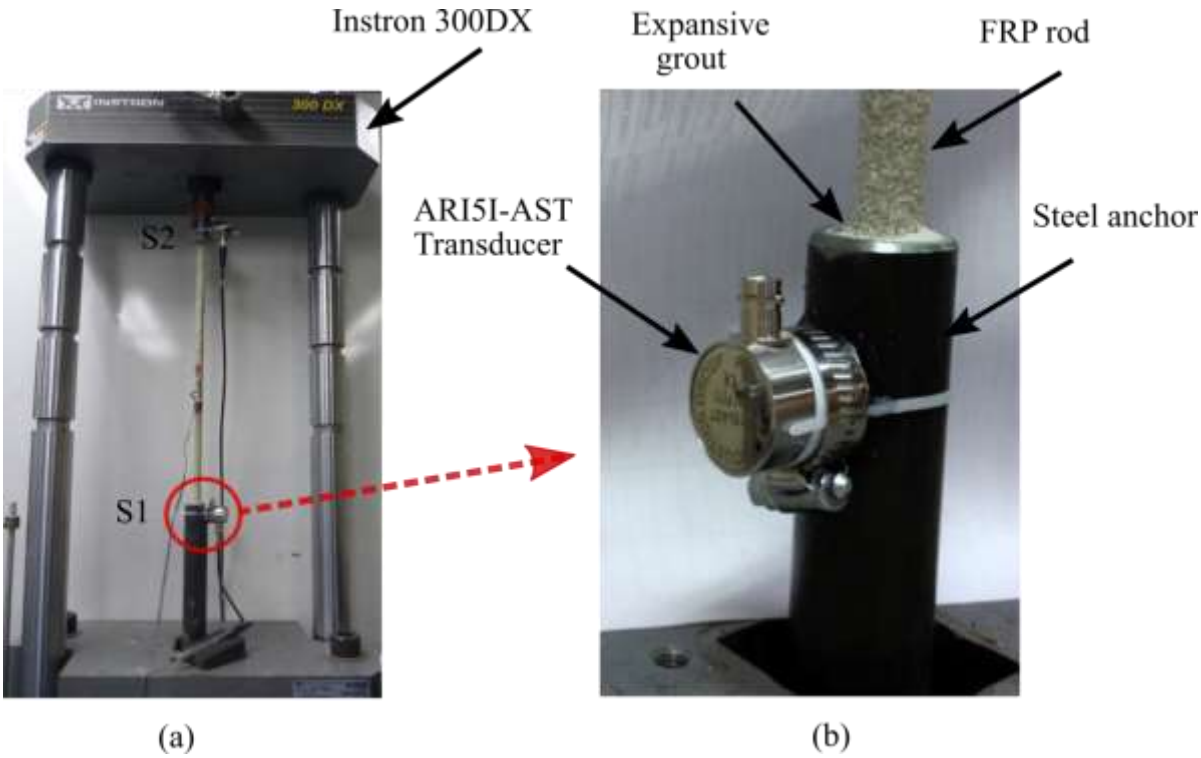

Figure 2. 1(a) Instron 300DX setup (b) Acoustic emission sensor

Studies on the glass and carbon FRP rods showed that AE signals from the glass and carbon FRP rods contain frequencies below 200 kHz [25]. Therefore, in this work resonant ARI5I-AST integral preamplifier piezoelectric sensor with operating frequency of 80 kHz to 200 kHz that had 40dB low noise preamplifier built in, from Mistras Physical Acoustic Corporation was used to detect emitted AE waves from the FRP rods. The conditioning and protection circuitry was designed for the sensors as in fig. 2.2 based on the data sheet of the sensors. The detected AE waves were sampled and stored using a USB Data Acquisition (DT9816-S, 16-bit) that had sampling frequency up to 750 kHz per channel.

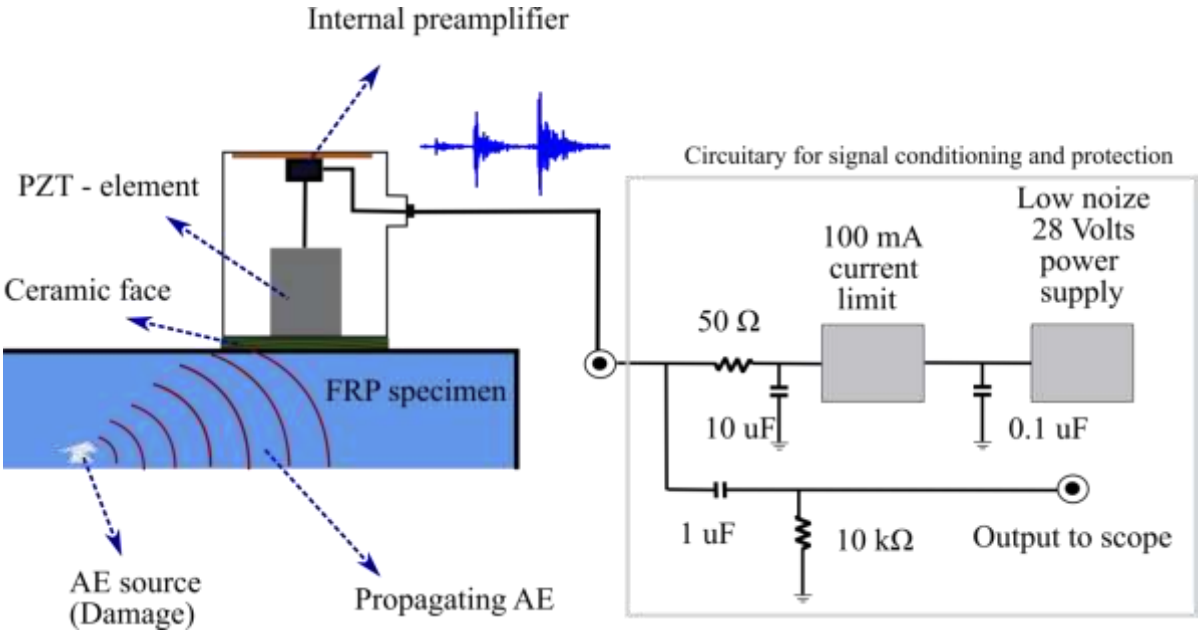

Figure 2. 2 Conditioning and protection circuitry for AST integral preamplifier piezoelectric sensor

2.2 Tensile test

Fig. 2.3 shows a schematic representing the tensile test setup. Initiating and progressing of damage generate acoustic emission waves that propagate inside the FRP rods and are sensed using the transducer. For the FRP rods, since they mainly consist of fibers, the main source

of AE generation is fiber breakage [25]. However, AE signal can be generated using other types of damages including matrix cracking and fiber-matrix debonding. For facilitating the transfer of AE waves to the transducer, the Proceq couplant gel (P.No. 71010031) was injected between the ceramic face of the sensor and the surface of the steel anchor. Studies showed that couplant gel can improve the transmission of AE waves to the AE sensor [26].

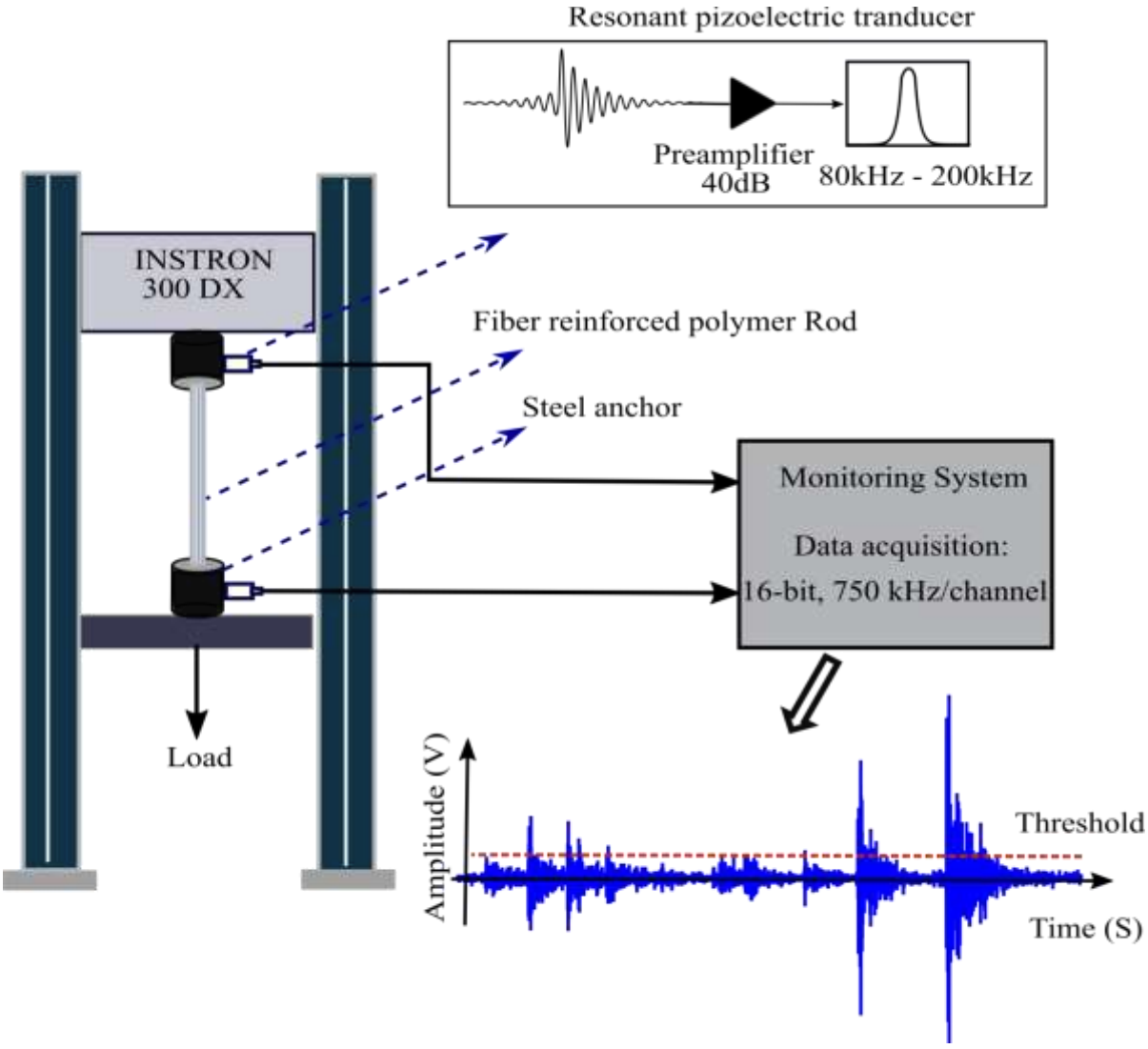

Figure 2. 3 Schematic of the AE experimental set up for FRP tensile test

Before applying the load the pencil-lead break tests were done for calibration of the sensor [27] and to set AE event detection algorithm's parameters. Using the testing machines,

ramping tensile load was applied to the test specimens until failure. The loading rate and displacement rate were calculated based on the CSA S806-12 standard. Table 2.1 represents the load information of each FRP rod.

Table 2. 1 FRP tensile test load information

Bar Type	No. specimens	Displacement Rate ($\frac{mm}{min}$)	Ultimate Load(kN)
CFRP size 2	3	0.8	78
CFRP size 4	2	1.8	250
GFRP size 4	2	4	117
GFRP size 6	2	6	240

2.3 Pencil-lead break test

Pencil-lead breaks (PLB) are extensively used to generate a reproducible artificial acoustic emission signal. This source is also referred to as the Hsu-Nielsen source. The PLB test consists of breaking a pencil lead with diameter of 0.5 mm (or 0.3 mm) and an approximate length of 3 mm by pressing that against the surface of the specimen [27]. Generated AE signals may totally be used for two purposes. First, they ensure that AE sensors are in a suitable contact with specimens for detecting the AE signals. Second, different parameters including attenuation and wave velocity can be determined. Moreover, in some studies the PLB tests were done to assess source location methods [28-29]. In this section the PLB test is used to find the attenuation in fiber reinforced polymer rods. The PLB apparatus used in this study is shown in fig. 2.4. To harmonize the PLB test the pencil is hold at the same angle to the FRP rod surface using ring shape foam. 15 places on the FRP rod (every five centimeter distance from sensor1 to sensor 2) are considered. For each place 6 pencil-lead break tests (more than one test) are done and the averages are used – see fig. 2.5-.

Figure 2. 4 Pencil-lead break test apparatus used in FRP test

For the sensor 1 and sensor 2 the AE signals can be stated as follows:

$$A_1 = A_s \times C_1 \times e^{-\alpha(L+x)} \qquad A_2 = A_s \times C_2 \times e^{-\alpha(L-x)} \qquad (2.1)$$

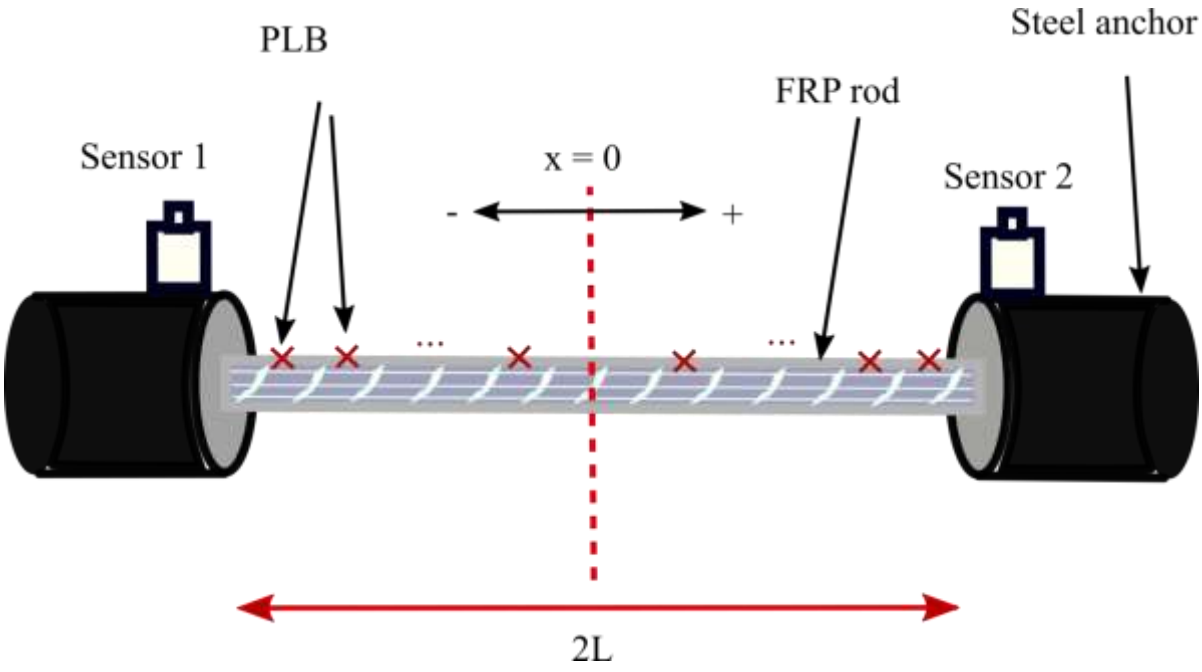

Figure 2. 5 A schematic of pencil-lead breaking test for attenuation measurement

Where A_s is the amplitude at AE source and C_i is used due to differences in coupling between sensor and material surface or in sensitivity of sensor.

To measure attenuation α the ratio of peak amplitudes detected at both sensors is evaluated for different AE sources (different places).

$$y_i = \ln(\frac{A_1}{A_2}) = \ln(\frac{C_1}{C_2}) - 2\alpha \times x_i \qquad (2.2)$$

Fig. 2.6 represents an example for the PLB test result. As it is shown in this figure, the peak amplitudes are used for attenuation measurements.

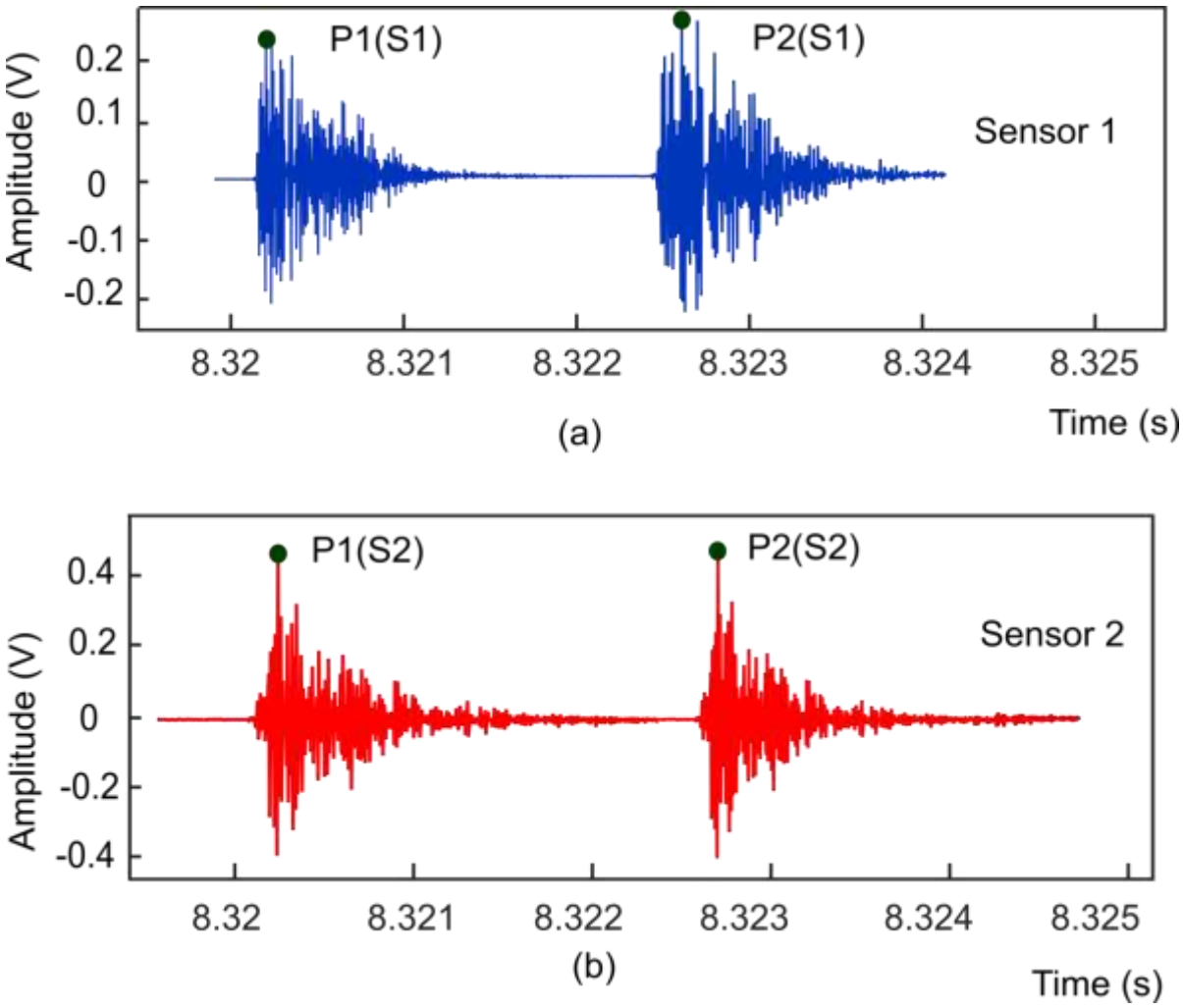

Figure 2. 6 Example of the PLB test result for both sensor at x= 25 cm

Table 2.2 lists the results of PLB tests measurement on the GFRP size 4 for different x. According to the equation (2.2) the slope of the y versus x can be used to find the attenuation. For this purpose the linear regression is used. Generally by having a set of data

(x_i,y_i) for i=1,2,…,n and a linear relation $y = a_0 + a_1x$, the coefficients a_0 and a_1 can be found as follows [30]:

$$a_1 = \frac{n\sum x_i y_i - \sum x_i \sum y_i}{n\sum {x_i}^2 - (\sum x_i)^2} \qquad a_0 = \bar{y} - a_1\bar{x} \qquad (2.3)$$

Fig. 2.7 represents the results for linear regression on the PLB data. Based on the equation 2.2 the attenuation is calculated from the slope of the regression line as 0.4296 dB /cm. The correlation constant of the regression is calculated using the formula in [30] as 0.9828.

Table 2. 2 PLB measurements data for GFRP rod size 6

x (cm)	A_1 (Volt)	A_2 (Volt)
-35	7.41	0.08
-30	2.22	0.07
-25	2.76	0.11
-20	0.92	0.11
-15	0.60	0.13
-10	0.39	0.13
-5	0.48	0.11
0	0.18	0.11
5	0.25	0.23
10	0.41	0.37
15	0.24	0.41
20	0.18	0.54
25	0.10	0.93
30	0.12	1.03
35	0.10	4.12

A correlation constant close to 1 state that the measurements follow the linear behavior as was expected in equation 2.2.

The above measurement is a good example of using PLB tests data. Moreover in the next chapter it will be explained that the PLB test can be used for setting parameters of AE event detection algorithms.

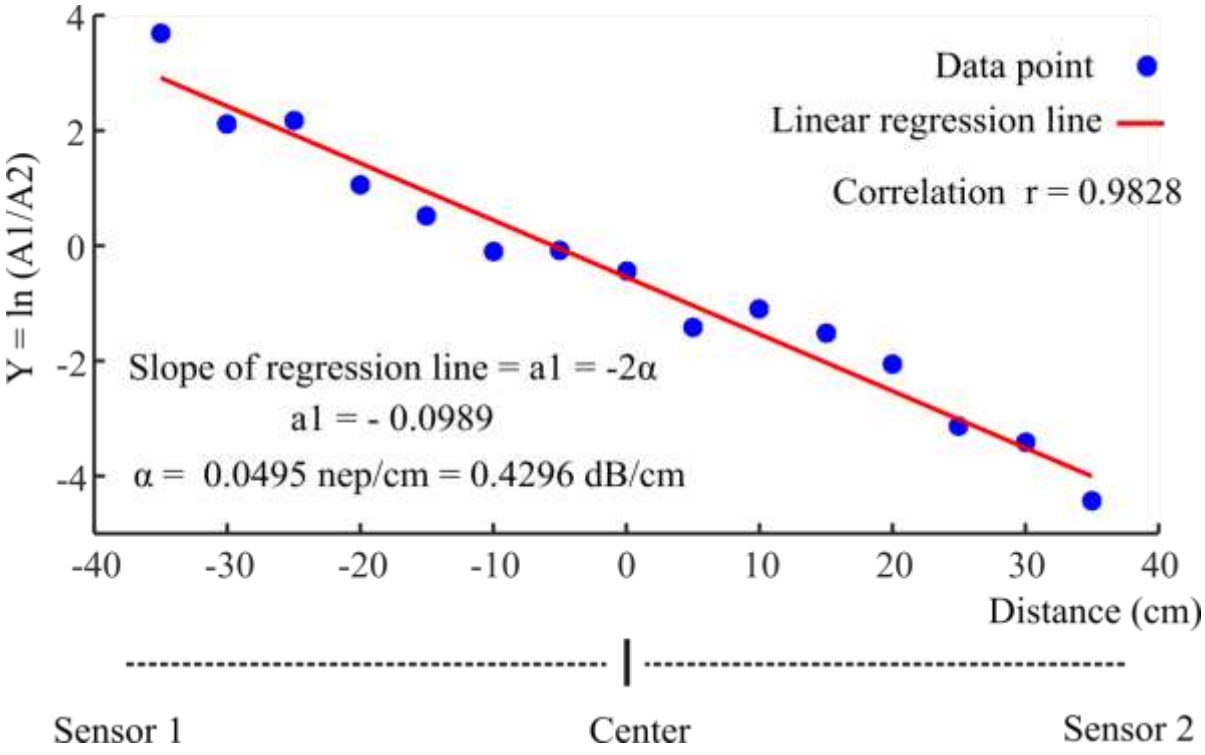

Figure 2. 7 Attenuation measurement using linear regression on the PLB tests data

CHAPTER 3: PATTERN RECOGNITION ANALYSIS FOR FAILURE PREDICTION

3.1. Introduction

This chapter presents a new robust method of failure prediction in FRP rods using acoustic emission (AE). In this chapter, at first we propose a new methodology called RMS (root mean square) algorithm, for detecting acoustic emission (AE) events come from progressive damage in fiber reinforced polymer (FRP) rods. The FRP rods used in tensile test are listed in table 1.1 and the load information for each rod is presented in table 2.1. A fuzzy c-means (FCM) clustering algorithm is used to classify these detected AE events into 3 clusters. Scanning electron microscopy (SEM) images of FRP rod cross-sections also show 3 types of damage. The main hypothesis in this study is that each cluster represents a damage mechanism. The number of events in each cluster is monitored versus the percent of ultimate load. The ratio of the number of AE events in one of the FCM clusters to the number of AE events in another FCM cluster was useful for predicting the failure of the FRP rods.

The content of this chapter was sent to a journal. For the FRP tensile test the FRP specimens and the scanning electron microscopy images are prepared by Maha Ghaib. The tensile experiments are done by Mohammadhadi Shateri and Maha Ghaib. The data are analyzed by Mohammadhadi Shateri.

3.2. Acoustic emission wave

3.2.1 AE features

Acoustic emission waves are transient stress waves due to material deformation. In other words, when sudden microstructural damage happens in material, elastic waves are generated by the rapid release of energy that propagates through the material [31]. The

vibrations are sensed through transducers that are mounted on the surface of the material. A data acquisition device captures signals from the transducer. The first step in the analysis of AE signals is the temporal isolation of AE events that are believed to have originated from each damage mechanism. For each discriminated AE event different features are estimated that are specified in fig. 1.5.

3.2.2 AE event detection algorithm

Most AE techniques for damage detection purposes use features of each AE event in an attempt to identify the type of damage mechanism, thus, a reliable AE event detection algorithm is needed. The threshold-based algorithm is used in the most commercial AE devices and most research work. In this work a new methodology called RMS algorithm is introduced, which offers decreased error rates compared to the threshold-based techniques. The results will show that unlike the threshold-based technique, the RMS algorithm can separate the AE event, even when the AE signal has strong burst events, and when two or more events are nearly coincident.

3.2.2.1 Threshold base algorithm

Threshold-based algorithm compares the AE signal with a threshold level (fixed or floating threshold). Whenever the AE signal passes the threshold for the first time, it is assumed that the AE event has started and then when it passes below the threshold again and remains under the threshold for a specific time, the AE event is completed. Three common parameters are used in this algorithm including hit definition time (HDT), hit lock time (HLT) and peak definition time (PDT). Fig. 3.1 represents how the parameters of this method are defined. The idea of this method is presented in [32]. The parameters of this method are selected using the pencil-lead break tests from different locations on the FRP rods. However, it is stated by Arumugam et al. [33] that the HDT parameter is selected using

trial and error since the proper value of this parameter guaranties the detection of a single AE event as only one AE event. Setting the HDT too high, will results in the loss of events. The main shortcoming with this technique occurs near failure where AE signals occur in strong bursts of nearly coincident events that never fall under the threshold. This technique will under estimate the number of events near failure.

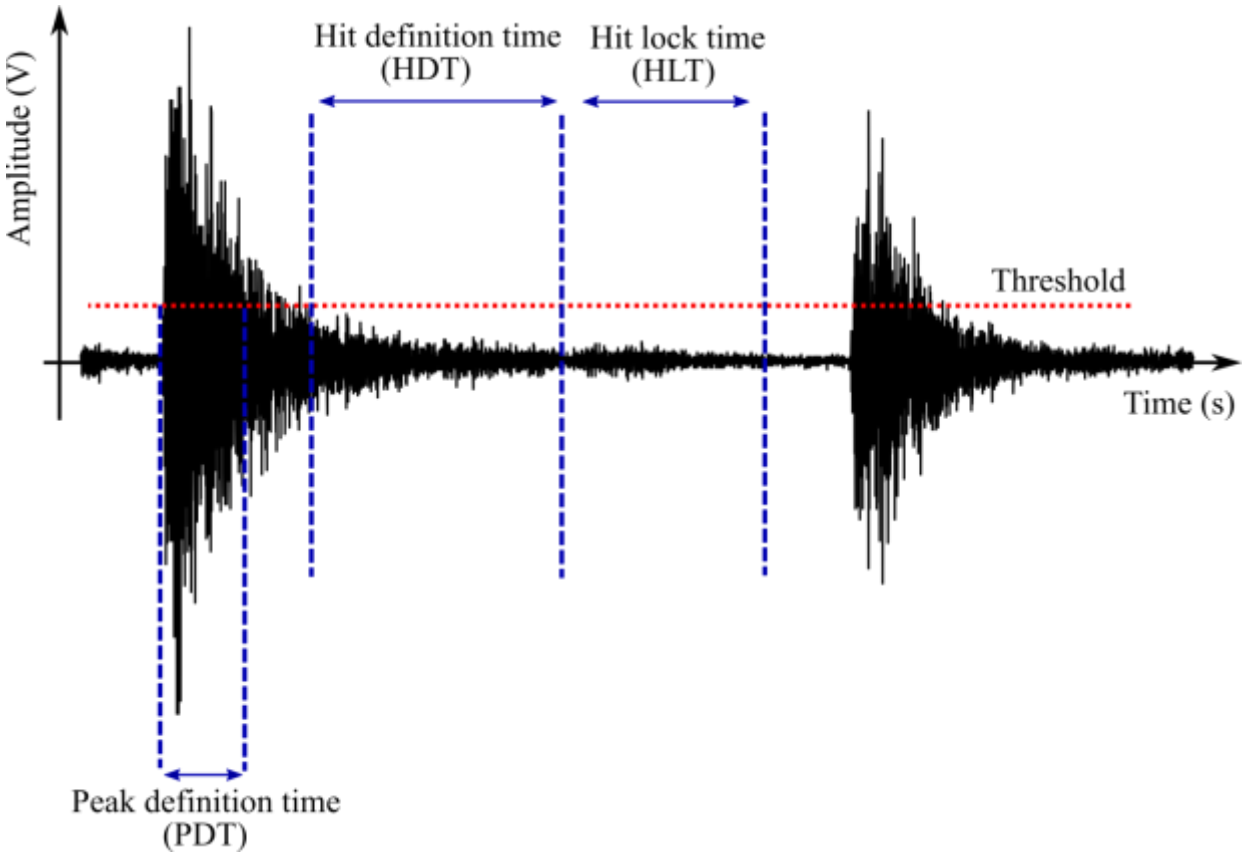

Figure 3. 1 Threshold based AE event detection algorithm parameters.

3.2.2.2. RMS AE event detection algorithm

An AE event detection algorithm that overcomes the two major problems with threshold-based technique is the RMS algorithm. The general idea of this method is similar to the methods stated in [34], however the details including parameters of algorithm and finding the optimum values for parameters are totally different. The idea of the RMS algorithm is

that it uses the information in the envelope of the AE signal that is found by root mean square of the AE signal. Using the RMS signal some intervals that have at least one event in them, are found. Then, a joint valley-peak finding algorithm with a floating threshold based on each pair of valley-peak is applied to them, which detects events separately. This algorithm is stated in three steps listed below:

- **STEP 1. Generating RMS signal with parameter N.**

  k^{th} Sample of the RMS signal can be founded by:

$$s_{rms}^{k} = \sqrt{\frac{(s_1^k)^2 + (s_2^k)^2 + \ldots + (s_N^k)^2}{N}}$$

- **STEP 2. Find an interval containing at least one event.**

  1. Apply fixed threshold F_{thr} to the RMS^N signal

     - If $(s_{rms}^{k} \leq F_{thr})$ and $(s_{rms}^{k+1} > F_{thr})$ then "s_{rms}^{k}" is the start point of the interval.

     - If $(s_{rms}^{k} > F_{thr})$ and $(s_{rms}^{k+1} \leq F_{thr})$ then "s_{rms}^{k+1}" is the end point of the interval.

  2. If in this interval the main signal has at least 'one' point above the main threshold M_{thr}, then it is a valid interval. Otherwise, back to the step 1.

- **STEP 3. Detecting the events that are in the interval**

  1. Find the pairs of Valley-Peak for RMS^N signal in each detected interval.

     - If $(s_{rms}^{k} < s_{rms}^{k-1})$ and $(s_{rms}^{k} < s_{rms}^{k+1})$, then "$s_{rms}^{k}$" is a valley.

     - If $(s_{rms}^{k} > s_{rms}^{k-1})$ and $(s_{rms}^{k} > s_{rms}^{k+1})$, then "$s_{rms}^{k}$" is a peak.

  2. Apply a floating threshold to each pair.

     - For a pair of (valley, peak), if $(\text{valley} < \text{Ratio} \times \text{peak})$, then it is called a valid pair.

3. For the valid pairs, the distance between each two series valley is defined as new interval such that each new interval represents an AE event.

4. Back to step 1.

Fig. 3.2 depicts a summary of the three step algorithm described above. In this algorithm three different kinds of parameters are used including threshold, RMS number, and Ratio. The M_{thr} is the main threshold and only those AE events that pass this threshold are detected. If it is set too large, then some events that come from the damage maybe missed and if it is set too small then some events that come from noise could be detected. This parameter has been selected as ten times of the noise level. The F_{thr} is the fixed threshold that is used to segment the raw data. It is applied to the RMS signal and most parts of RMS signal comes from the noise, thus this threshold is considered to be a few times of the noise level. The RMS number N is used for finding the envelope of the AE signal. If N is selected too large, then those AE events with small duration maybe missed. The expected minimum duration of AE event can be found using pencil break test. Thus, the value of N can be selected as the minimum duration divided by sampling time. The last parameter is the Ratio that is a floating threshold. It is used for deciding if a pair of valley-peak is considered as an event or not. It can be proved (See appendix) that the Ratio can be found as follow:

$$\text{Ratio} = \frac{M_{thr} + 3F_{thr}}{2(M_{thr} + F_{thr})} \qquad (3.1)$$

3.3. Pattern recognition technique for clustering AE waves

3.3.1. Multi-feature AE analysis

The multi-feature AE analysis uses AE features such as peak amplitude, duration, energy, etc. to discriminate the different damage mechanisms in FRP rods. It should be noted that in this study the peak amplitude is used in dBVolt based on 3.2 as follows [8]:

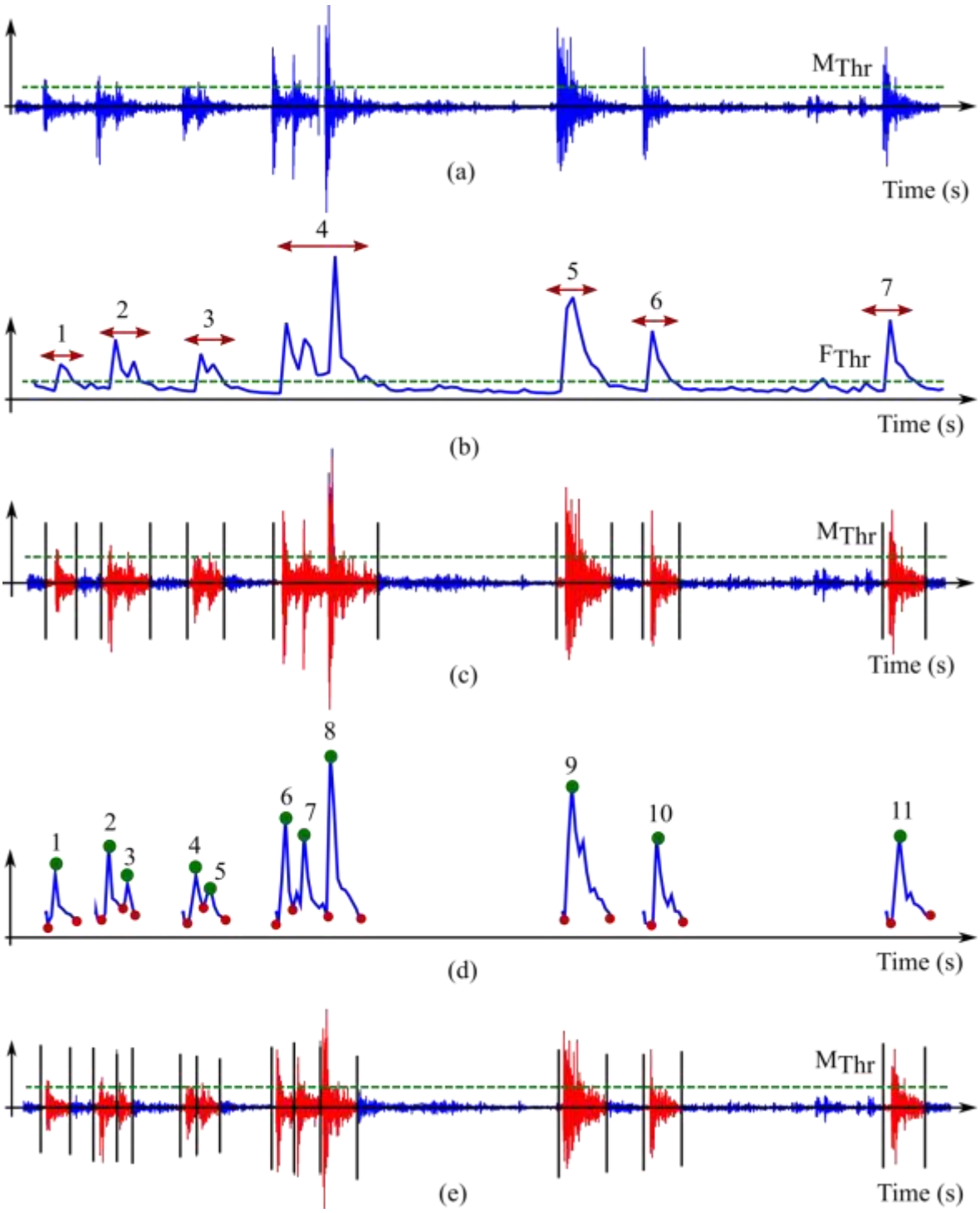

Figure 3. 2 Step by step representation of the RMS AE event detection algorithm (a) Main AE signal from sensor with the main threshold (b) RMS signal with fixed threshold (c) Main signal with the intervals that each contains at least one AE event (d) Valley-peak pairs in each interval that represent an AE events (e) Detected events

$$P_{dBV} = 20 \times \log_{10}(P_V / 1uV) - 40dB \quad (3.2)$$

Where 40 dB is the gain of the sensor and 0dBV corresponds to 1uV at the input port of sensor. Here, by using unsupervised pattern recognition analysis (Fuzzy C-means combined with principle component analysis) based on the time-based features discussed earlier, the AE events are clustered. In this work four features are selected and they are peak amplitude, energy, duration and number of count of each detected AE event. These time-based features have been used commonly in studies [16,35] for clustering AE events. In this study the FCM method based on the time-based features of AE events is used to define clusters. For the clustering purpose, each of these features is non-dimensionalised by its maximum value so that it falls in between zero and one [14].

3.3.2. Fuzzy C-means (FCM) algorithm

FCM is an unsupervised clustering algorithm proposed by Bezdek [36] that partitions the input data set into C fuzzy clusters. The key point here is that the similarity of each data point with each cluster is represented as a value between zero and one that is called the membership degree (probability). Let p be the number of features (here is four) collected from N detected AE events and $y_k (k = 1,2,...N)$ be the input pattern vectors thus, $Y = [y_1, y_2, ...y_N]^T_{N \times P}$ is the input matrix. The FCM uses fuzzy partitioning so that each input pattern vectors $y_k (k = 1,2,...N)$ belongs to each cluster with different membership degree $u_i(y_k), i = 1,2,...,C$. The optimal values for membership degrees and centers are iteratively founded by minimizing the objective function J_m:

$$J_m(U,V) = \sum_{k=1}^{N} \sum_{i=1}^{C} [u_i(y_k)]^m \| y_k - v_i \|_A^2 \quad (3.3)$$

Where:

- $V=(v_1,v_2,...,v_C)=$ matrix of centers, $\|.\|_A=$ Induced A-norm on $\mathbb{R}^N$
- $d^2(y_k,v_i)=\|y_k-v_i\|_A^2=(y_k-v_i)^T A(y_k-v_i)=$ Square distance between k-th input pattern data y_k and i-th center v_i. $A=$ positive definite ($N\times N$) weight matrix
- $m=$ weighting exponent $1\le m\le\infty$
- $U=\begin{bmatrix} u_1(y_1) & \cdots & u_1(y_N) \\ . & . & . \\ . & . & . \\ . & . & . \\ u_C(y_1) & \cdots & u_C(y_N) \end{bmatrix}=$ Membership matrix where $u_{i(y_k)}$ is the membership degree of the k-th pattern vector y_k in the i-th cluster such that $\sum_{i=1}^{C}u_{i(y_k)}=1 \quad \forall k$.

By considering A as the identity matrix ($\|.\|_A=$ Euclidian norm) the minimization of $J_2(U,V)$ is resulted in the following two updating rules for the centers and membership matrix:

$$v_i=\frac{\sum_{k=1}^{N}[u_{i(y_k)}]^m y_k}{\sum_{k=1}^{N}[u_{i(y_k)}]^m} \quad ; i=1,2,...,C \qquad (3.4)$$

$$u_{i(y_k)}=\left[\sum_{j=1}^{C}\left[\frac{d(y_k,v_i)}{d(y_k,v_j)}\right]^{\frac{2}{m-1}}\right]^{-1} \quad ; k=1,2,...,N;\ i=1,2,...,C \qquad (3.4)$$

3.3.3. Optimum number of clusters

One very important parameter I n the FCM algorithm is the number of clusters (C). The process of determining number of clusters, aims at finding the C in such a way that provides maximum compactness for each cluster and also maximizes the distance between each two cluster centers [37]. To this end, different cluster validity indexes based on compactness and separation of fuzzy clusters are defined in [37-40]. In this experiment three indexes

including partition coefficient (PC) [38], partition index (PI) and SC index [39], and Xie and Beni index (XB) [40] are proposed.

Partition coefficient (PC) is a measure of overlapping between the clusters and its value is between zero and one. As the value of this index is near to one it means the degree of cluster overlapping is smaller .Thus, the optimum number of clusters makes this value maximum. This index is defined as follows [38]:

$$PC(C) = \frac{1}{N}\sum_{i=1}^{C}\sum_{k=1}^{N}[u_i(y_k)]^2 \quad (3.5)$$

Partition index (PI) provides a measure of compactness of each cluster in its numerator and the separation of the clusters in its denominator. Therefore, the optimal number of clusters gives the minimum value of this index. This index is defined as follows [39]:

$$PI(C) = \sum_{i=1}^{C}\frac{\sum_{k=1}^{N}[u_i(y_k)\,]^2 d^2(y_k, v_i)}{\sum_{k=1}^{N} u_i(y_k)\sum_{j=1}^{C} d^2(v_j, v_i)} \quad (3.6)$$

The SC index provides a measure of compactness of each cluster in its numerator and the separation of the clusters in its denominator. Therefore, the optimal number of clusters gives the minimum value of this index. This index is defined as follows [39]:

$$SC(C) = \sum_{i=1}^{C}\frac{\sum_{k=1}^{N}[u_i(y_k)\,]^2 d^2(y_k, v_i)}{\sum_{k=1}^{N} u_i(y_k)\sum_{j=1}^{C} d^2(v_j, v_i)} \quad (3.7)$$

Xie and Beni index (XB) like the PI index gives a measure of compactness and separation in its numerator and denominator respectively; but uses the minimum distance between the centers as a measure of separation. The optimum number of clusters makes this value maximum. This index is defined as follows [40]:

$$XB(C) = \frac{\sum_{i=1}^{C}\sum_{k=1}^{N}[u_i(y_k)\,]^2 d^2(y_k, v_i)}{N \times min_{i\neq j} d^2(v_j, v_i)} \quad (3.8)$$

3.4. Failure prediction using pattern recognition

3.4.1. Comparison of AE events detection algorithms

In this study, a sampling frequency of 400 KHz was considered for the data acquisition system. The main threshold M_{thr} for both techniques was set according to the level of the noise, to 0.02v (approximately ten times greater than the noise level).

Using this main threshold and by assigning a minimum limit to number of AE samples for each event (20 samples for this experiment) the noise signals were filtered. Some of these signals considered to be AE signals coming from cracking of the grout in the grips that were characterized as short duration and small amplitude AE events. For the threshold-based algorithm, the value of HDT was selected as 125us using pencil-lead break test. Then using trial and error method [33] the value of HDT was changed between 75us and 150us. Results showed that for the AE data in this experiment, the threshold based method can detect more separate single AE events using HDT equal to 100us. An appropriate selection of the HDT is important since can ensure that a single AE event is detected as only one event. The HLT parameter typically considered as 300us. For the RMS algorithm, the F_{thr} was set according to the noise to 0.005 volt (two and half times of the noise level). By having M_{thr} and F_{thr} and using equation (3.1), the Ratio can be calculated to be 70%. Using the pencil-lead break test and by considering sampling frequency, the RMS number N was selected as 50 samples. The two AE event detection techniques were applied to the same AE data set from FRP rod tensile tests listed in table 1. Fig. 3.3 demonstrates an example of the results of these two methods. The first two AE events in this figure are nearly coincident since they occur consecutively in less than the 100 us (HDT value). Moreover, the second event is a strong burst event since it tends to have threshold crossing until the next AE event occur. From the fig. 3.3 it can be seen that unlike the threshold-based technique, the RMS algorithm can

separate the AE event, even when the AE signal has strong burst events, and when two or more events are nearly coincident.

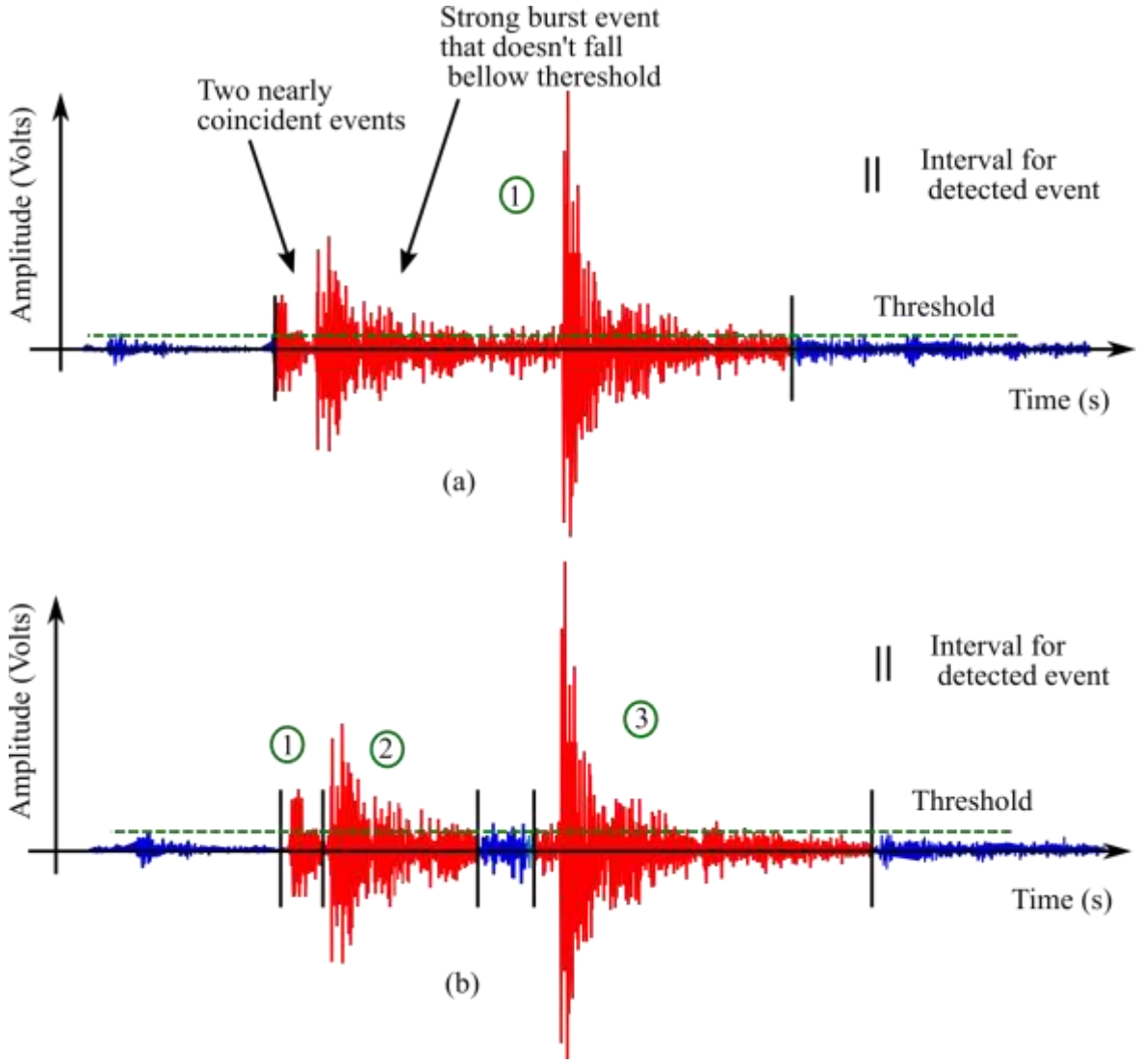

Figure 3. 3 An example of performance of the detection algorithms. (a) Threshold based algorithm (b) RMS Algorithm.

The RMS method uses the pair of peak-valley in the envelope and therefore is not sensitive to the distance between two consecutive Ae events. To better compare these two techniques, FRP tensile test was divided into three regions based on the percentage of the ultimate load. For example for the CFRP size 2 the tensile test was discriminated into three parts (0 - 26) kN, (27 - 52) kN, and (53 - 78) kN based on the ultimate load 78kN. For each part some data

files were selected randomly. This random selection contained 4180 AE events. Each of these events was analyzed by hand to determine the true number of events. For each algorithm missing an AE event or counting multiple AE events as a single AE event, was considered as error in AE event detection. The performance of the AE event detection algorithms is listed in table 3.1. As the table 3.1 shows, for the threshold based algorithm the amount of error increases from the middle of the test to the end of the test because the events in these regions are very close to each other and this algorithm is not able to detect them separately. However, the RMS algorithm uses the envelope of the AE signal and the variation in that, thus it is not affected by the distance between the AE events.

Table 3. 1 An example of the error in two AE event detection algorithms for CFRP size2 (the tensile test is divided into three parts according to the amount of the load)

Error / Method	Start of the Test (0 - 26) kN	Middle of the Test (27 - 52) kN	End of the Test (53 - 78) kN
Threshold Algorithm	0% (0 in 15 events)	10.3% (77 error in 746 events)	15.6% (533 error in 3419 events)
RMS Algorithm	0% (0 in 15 events)	6.6% (49 error in 746 events)	7.8% (265 error in 3419 events)

Another advantage of RMS algorithm over threshold based method is that for the threshold based algorithm the only way for choosing the HDT is trial and error. On the other hand, in the RMS algorithm all the parameters can be selected reasonably using pencil-lead break test.

3.4.2. Damage characterization in FRP rods using multi-feature analysis of AE data

The multi-feature analysis was applied to discriminate AE events based on the four features that are duration, peak amplitude, energy and number of counts. The main hypothesis in this study was that each cluster represented a damage mechanism [16]. The time-based features were extracted by the RMS algorithm. The different cluster validity indexes PC, PI and SC were applied to determine the number of clusters for each data set (see fig. 3.4).

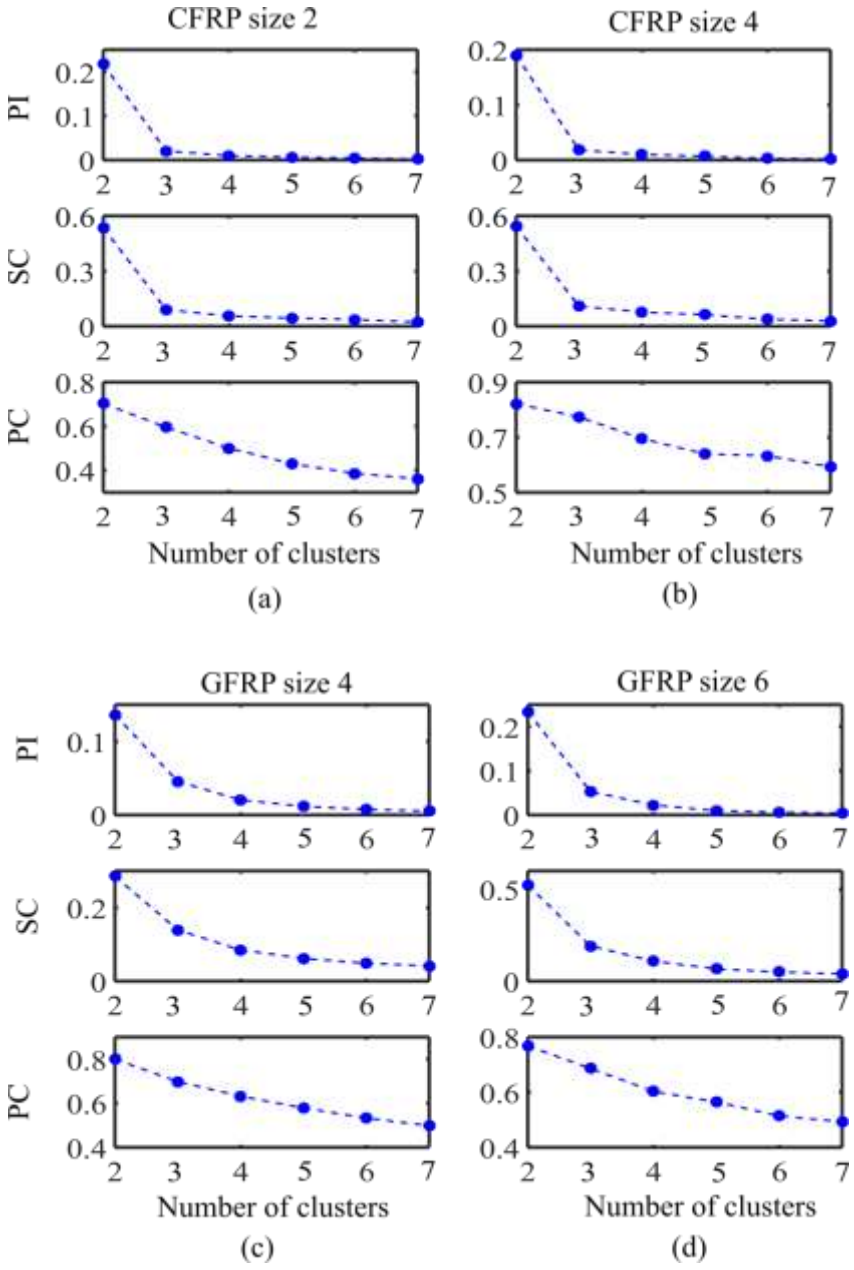

Figure 3. 4 Cluster indexes criteria applied to AE data sets

The optimum number of clusters should provide minimum values for PI and SC indexes and at the same time give maximum value for the PC index. The PC index measures the amount of overlapping between the clusters and its value at the optimum number of clusters shouldn't be too far from 1. Form the fig. 3.4 the number of clusters is determined as three for all the rods. The scanning electron microscopy (SEM) of tested FRP rods in fig. 3.5 shows three types of damage, which is consistent with the three clusters in the AE data. It means the SEM images substantiate the method used to define the clusters. Therefore, in the FCM method, three clusters were used. The results of clustering are presented in fig. 3.6. All the four parameters that were used in the FCM clustering are plotted versus the time and the colors indicates the clusters. From the fig. 3.5 it can be seen that the AE data sets are well discriminated into the clusters. The first cluster for all the rods contains the largest number of AE events and it starts from the beginning of the test until the failure. This cluster contains the smallest time-based features. The third cluster includes the smallest number of AE events and mostly starts at the middle stages of load.

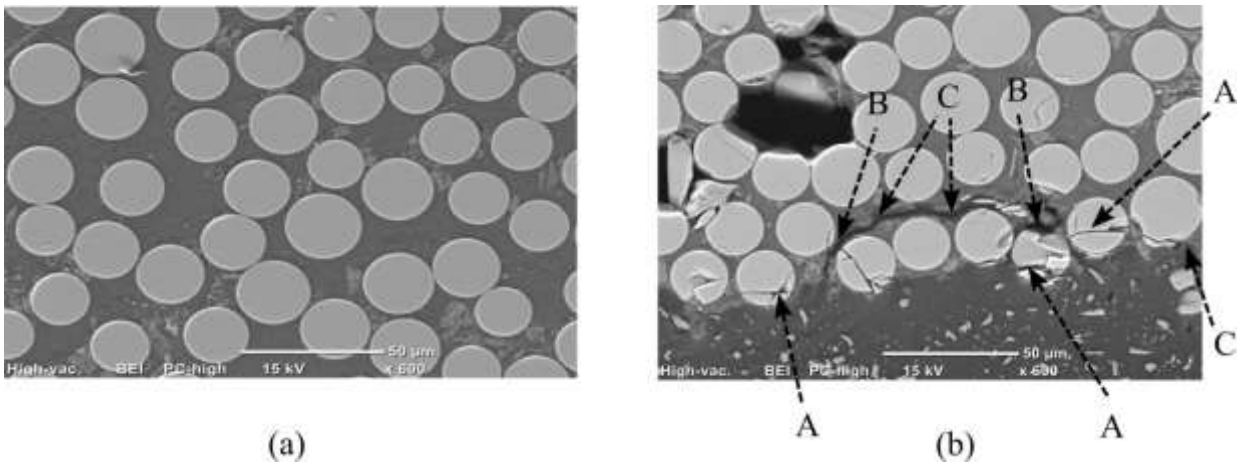

Figure 3. 5 Scanning electron microscopy (SEM) image of FRP rod (a) untested (b) after tensile test, A, B and C refer to the fiber breakage, fiber-matrix debonding and matrix cracking, respectively.

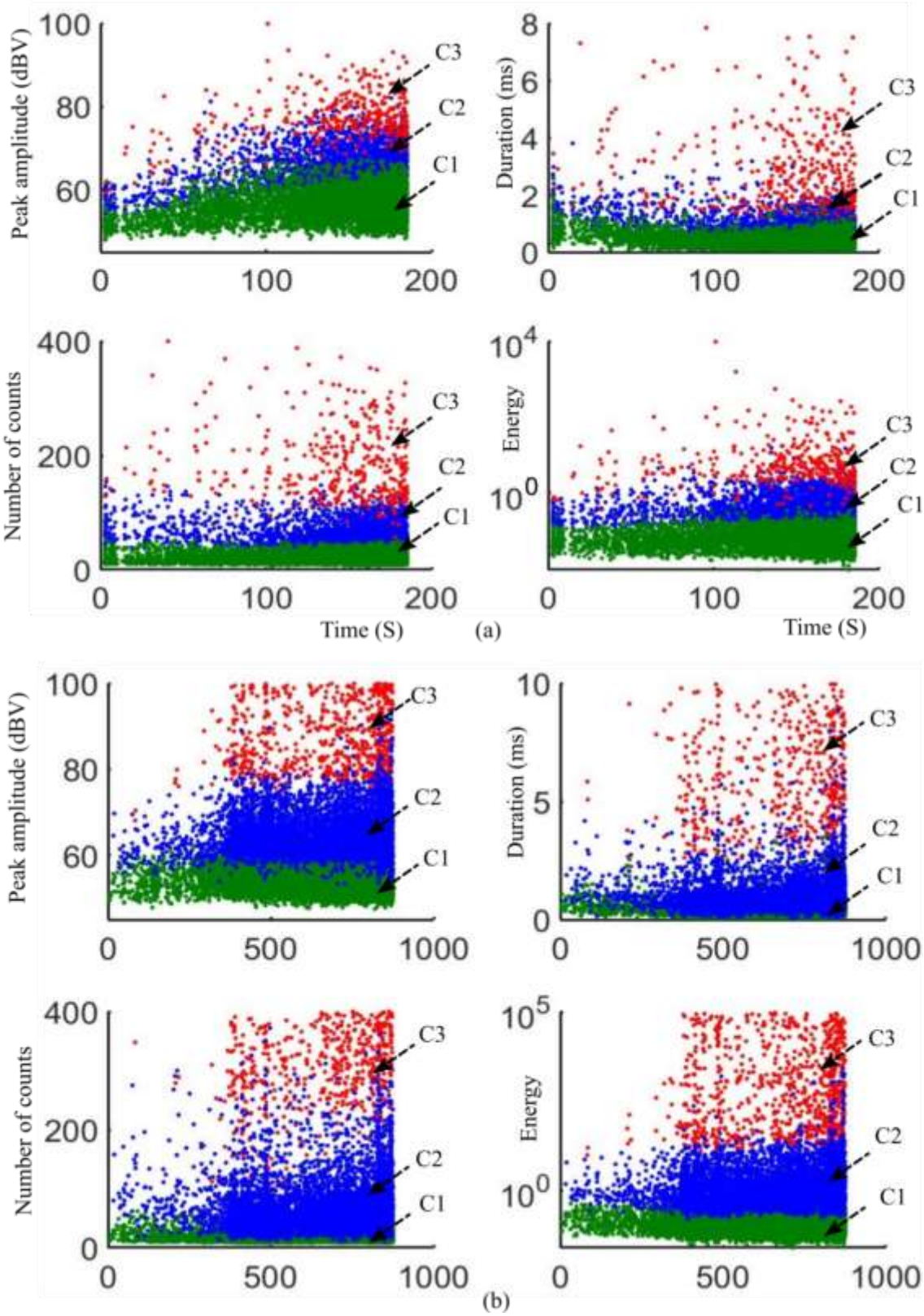

Figure 3. 6 Clustering results of the AE data set for the FRP rods using fuzzy c-means clustering algorithm (a) GFRP size 4 and (b) CFRP size 2.

This cluster contains the largest values of time-based features that refer to the strong AE events. In the next section the first cluster and the third cluster are used for prediction of the failure in FRP rods. For a better quantifying the clusters based on the time-based features, the clusters are characterized in the table 3.2.

Table 3. 2 Characterization of clusters using time-based features for all the FRP specimens

Bar Type	Cluster		No. of Events	Amplitude (dBV)	Duration (ms)	No. of Counts	Energy ($Volt^2$-usec)
CFRP size 2	C1	First specimen	23598	48 - 59	0.05 - 2.5	< 50	< 0.45
		Second specimen	23146	49 - 61	0.05 - 2	< 50	< 0.47
	C2	First specimen	9144	56 - 78	0.3 – 3.5	20 - 250	0.2 - 22
		Second specimen	8212	58 - 77	0.8 – 3.3	40 - 230	0.35 – 17.5
	C3	First specimen	1190	77 - 100	> 3 Contains large values	> 200	> 21.5 Contains large values
		Second specimen	850	75 - 100	> 3 Contains large values	> 200	> 22.5 Contains large values
GFRP size 4	C1	First specimen	25906	48 - 62	0.07 - 1.1	< 40	< 0.4
		Second specimen	21489	49 - 61	0.08 – 0.8	< 35	< 0.45
	C2	First specimen	21231	59 - 75	0.4 - 2.2	30 - 120	0.25 - 7
		Second specimen	12934	55 - 70	0.3 - 1.5	25 - 90	0.20 - 6
	C3	First specimen	9440	74 - 100	> 1.5 Contains large values	> 110	> 5 Contains large values
		Second specimen	5651	68-100	> 1.2 Contains large values	> 85	> 3.8 Contains large values

From the table 3.2 it can be seen that for FRP specimens from the same type each cluster can be characterized with a certain ranges of AE features. It suggests that the determined ranges of features can be applied to other same type of FRPs to discriminate AE events into clusters without using other clustering algorithm.

3.4.3. Predicting failure using clustered AE data

The procedure that is stated here for predicting the failure in the FRP rods is based on the activity of the clusters. The number of AE events in the first cluster and the third cluster were monitored in different percent of ultimate load. A new parameter named Ratio Pattern is defined in 3.5 as the ratio of the number of AE events in the third cluster to the number of AE events in the first cluster. As it was mentioned in the table 3.2, the third cluster is characterized by the strong AE events, i.e. AE events with higher energies, larger peak amplitudes, durations and number of counts. This kind of AE events might be the results of the fiber pull-out which were observed mostly toward the end of the test. The fig.3.6 shows that these strong AE events have lower density at the beginning of the test and larger density toward the end of the test. The fiber-matrix debonding can result in fiber pull-out and increasing the number of fiber pull-out can lead to final collision/failure. Therefore, the Ratio Pattern defined to find when the number of these strong AE events increase severely compare to the other AE events. Fig. 3.7 shows the cumulative Ratio Pattern for the GFRP and CFRP rods in different percent of ultimate load.

$$\text{RatioPattern} = \frac{\text{Number of AE event in the last cluster}}{\text{Number of AE event in the first cluster}} \qquad (3.5)$$

They are normalized to their maximum values. It can be seen that around 40% of the ultimate load for GFRP rods and 60% of the ultimate load for the CFRP rods, the slope

changes almost by factor of 10 and then the slope remains almost constant until the failure. This evolution of cumulative Ratio Pattern indicates that the number of AE events in the third cluster compared with number of AE events in the first cluster increases notably and then this ratio stands almost constant until the failure. In other words, if each cluster is assigned to a specific damage mechanism [16], then the fast increase in the number of AE events in the third cluster indicates fast growth of the third type of the damage mechanism that ultimately leads to the rod failure. These thresholds can be compared to the standard CAN/CSA-S6-06, and CAN/CSA-S806-02, where the maximum permissible stresses in GFRP and CFRP tendons are 25% and 65% of the ultimate load. Therefore, the ratio pattern can be used to predict when the rods are nearing their maximum permissible stress levels.

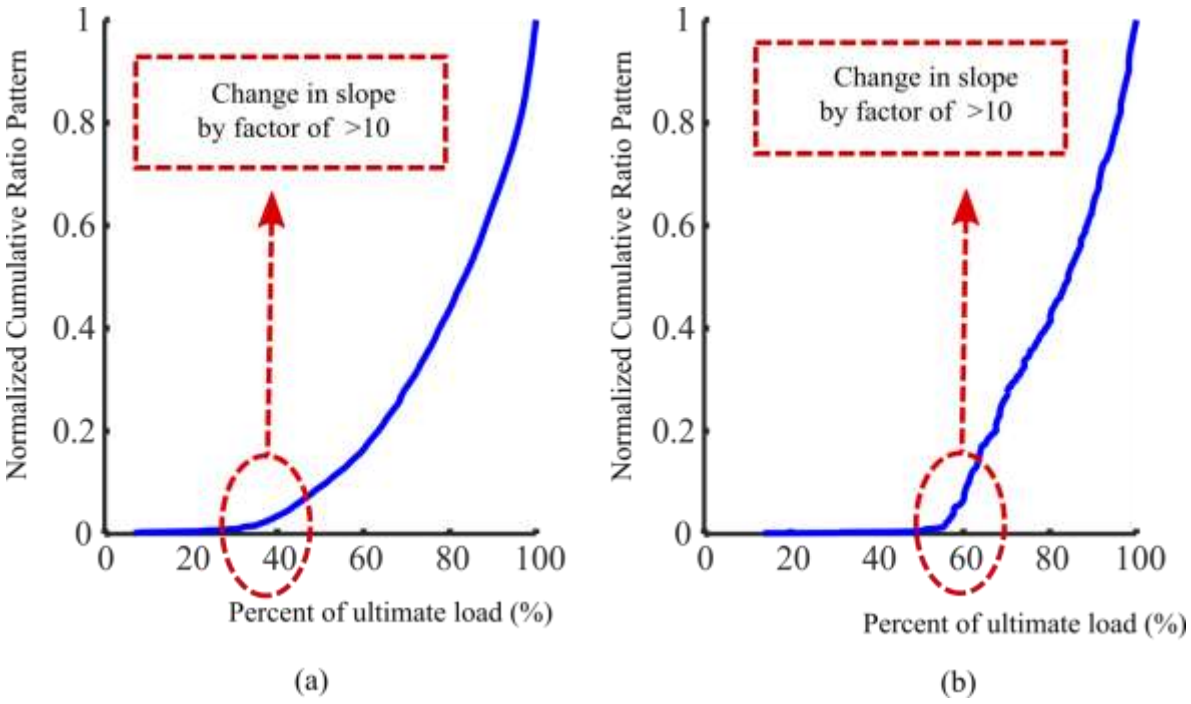

Figure 3. 7 Normalized cumulative Ratio pattern versus the percent of ultimate load (a) GFRP rod size 4 (b) CFRP rod size 2

The Ratio Pattern method was further tested by using it for failure prediction rods that were not part of the original set of rods used to determine the clusters. One was a CFRP rod and

one was a GFRP rod. As it was mentioned in the last section, for each type of FRPs, each cluster is characterized with a certain ranges of AE features. In this test the average of the limits in table 3.2, was used to define the clusters used in the analysis of the AE signals from rods that were not part of the tests summarized in Table 3.2. The result of applying Ratio Pattern to these FRPs is presented in Fig.3.8.

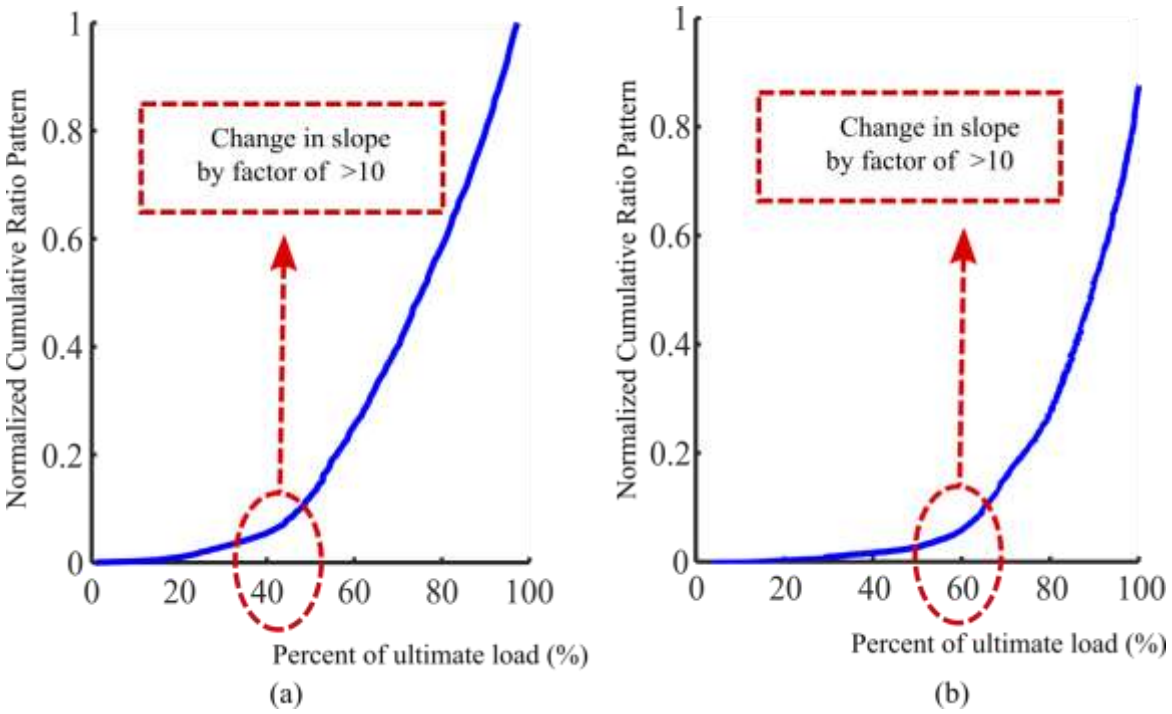

Figure 3. 8 Normalized cumulative Ratio pattern versus the percent of ultimate load for the clustered AE events based on table 4 (a) GFRP rod size 4 (b) CFRP rod size 2

Similar to the Fig.3.7 it can be seen from Fig. 3.8 that around 40% of the ultimate load for GFRP rods and 60% of the ultimate load for the CFRP rods, the slope changes almost by factor of **1**0 and then the slope remains almost constant until the failure. This severe change in slope which is referred to the onset of strong AE events (strong damage) is suggested to be used for providing warning about the impending failure.

CHAPTER 4: FREQUENCY ENTROPY METHOD FOR FAILURE PREDICTION

4.1. Introduction

This chapter presents a new robust method using acoustic emission (AE) entropy to determine when the maximum recommended load of FRP rods is exceeded. According to the CAN/CSA-S806-12 standard, the maximum recommended stress in FRP bars under service loads should not exceed 25% and 65% of the ultimate strength for glass FRP (GFRP) and carbon FRP (CFRP), respectively. ACI440.1R recommends that these limits be 20% and 55% for GFRP and CFRP, respectively. These stress values are set to prevent creep failure in FRP bars. However, for in-service applications there are few physical indicators that these values have been reached or exceeded. In this work analysis of acoustic emission (AE) signals is used to determine when the stress in FRP bars has exceeded certain threshold values. The hypothesis is that if the threshold values of stress determined for a given bar are higher than the values recommended by the codes for sustained load, the bar will safely carry the sustained stress throughout the service life of the structure. On the other hand, if the threshold values from the AE test are lower than the code recommended values for sustained stresses, the bars in question will need to be further tested under sustained load to confirm their safe use in service. The threshold value will be referred to in this paper as the value of recommended stress, or load. In this study, histograms of the AE signal entropy are used to monitor damage progression in FRP bars. Entropy is defined in the frequency domain using Fourier transform/wavelet transform of each detected AE events. Entropy is a measure of the randomness of AE signals or how uniformly the energy is distributed in frequency. More uniform distributions have higher entropy. As damage increases, more events are expected to occur that are the result of simultaneous independent damage

mechanisms. If different damage mechanisms are simultaneously present on AE event, then energy would be expected to be spread more uniformly over frequency. Therefore, the AE entropy is expected to raise as the damage in FRP bars progresses. The threshold for high entropy AE events was set using the one-sided Chebyshev's inequality with parameter k=2 and the histogram of AE entropy measured at 10-15% of ultimate load. AE events that are greater than two standard deviations above the mean are classified as high entropy events. According to one-sided Chebyshev's inequality whenever more than $\frac{1}{1+k^2} \times 100\%$ (20% for k=2) of AE events have high entropies, a new distribution of high entropy AE events is assumed to exist. Monitoring high entropy AE events provide a useful warning when the maximum recommended load of the FRP rods has been exceeded.

The content of this chapter was sent to a journal. For the FRP tensile test the FRP specimens are prepared by Maha Ghaib. The tensile experiments are done by Mohammadhadi Shateri and Maha Ghaib. The data are analyzed by Mohammadhadi Shateri.

4.2. Acoustic emission entropy

The Shannon entropy or information entropy that was proposed by Shannon [41] is a measure of randomness or uncertainty of a random variable. Let X be a random variable with distribution function Pr(x), where $x \in \{x_1, x_2, \dots, x_M\}$ and $\sum_{i=1}^{M} \Pr(x = x_i) = 1$. The Shannon entropy for the random variable X is defined as follows:

$$\mathrm{H(X)} = -\sum_{\mathrm{i=1}}^{\mathrm{M}} \mathrm{Pr(x = x_i)\log(Pr(x = x_i))} \qquad (4.1)$$

For each AE event detected using RMS technique (See chapter 3) during the tensile test of FRP rods, the frequency content can be considered as a random variable where its probability function is defined as the frequency spectrum normalized by the total magnitude

of spectrum [23]. Therefore, the Shannon entropy in (4.1) can be used to find the entropy of acoustic emission signals (See Fig. 4.1).

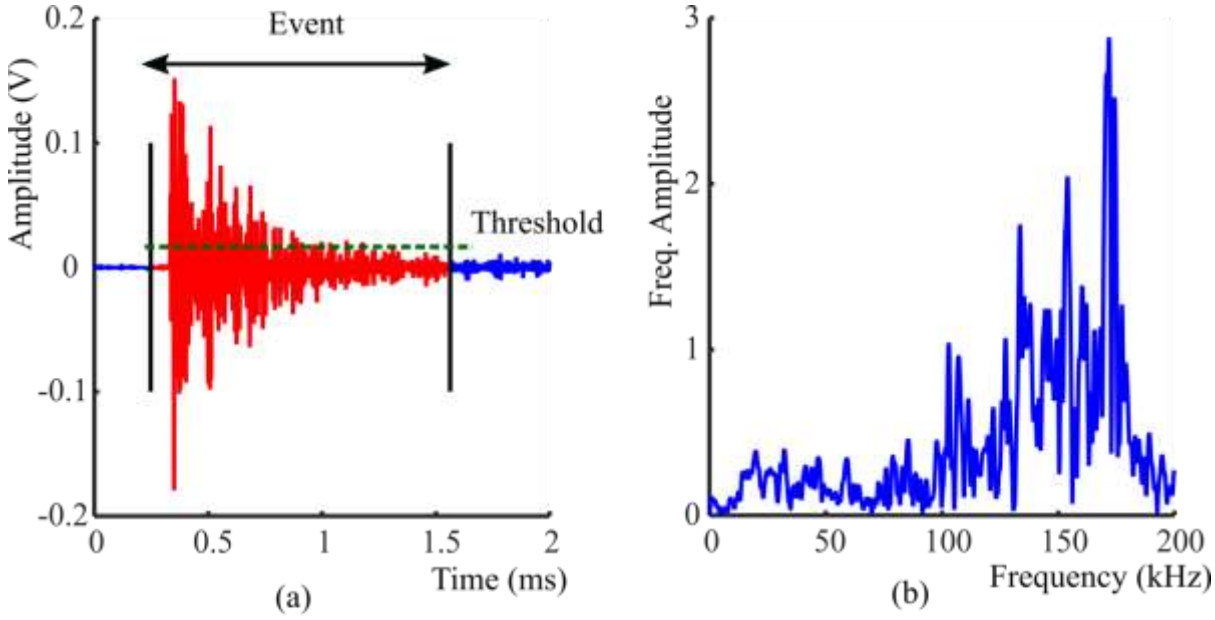

Figure 4. 1 AE entropy calculation (a) Detected AE event using RMS algorithm (b) Frequency spectrum of AE event (c) Applying the Shannon entropy formula to the normalized spectrum.

In this sense the acoustic emission entropy represents a measure of uncertainty about the energy distribution in different frequencies. In other words, if the energy of acoustic signal is distributed in a few frequencies the entropy is small; on the other hand large entropy is expected when the energy is distributed in more frequencies. In this study the entropy of acoustic signal is defined using Fourier transform and Wavelet transform that are explained below.

4.2.1 Acoustic emission entropy using Fourier transform

For a sequence of N samples of a signal $\{x_1, x_2, \dots, x_N\}$ the discrete Fourier transform (DFT) is defined as follows [42]:

$$X_k = \sum_{n=0}^{N-1} x_n e^{-j2\pi kn/N} , \qquad k = 0, 1, \dots, N-1 \qquad (4.2)$$

Where $\{X_k\}, k = 0, 1, \dots, N-1$ are the DFT coefficients or frequency samples of signal x_n. According to the Shannon entropy (4.1) for computing entropy the probability function needs to be defined in frequency. For a pure real signal x_n the DFT is symmetric i.e. $X_{N-k} = X_k^*, k = 0, 1, \dots, N-1$ where * means complex conjugation [42]. Therefore, using the first half of DFT coefficients (positive frequencies) the probability function in frequency domain can be defined as follows [22]:

$$\Pr(X = X_i) = \frac{|X_i|}{\sum_{j=0}^{\frac{N}{2}-1} |X_j|} \qquad i = 0,1, \dots, \frac{N}{2} - 1 \qquad (4.3)$$

where $|X_i|$ is the magnitude of signal in the i-th frequency.

It should be noted that by considering $N = 2^l$ where l is an integer, the DFT (4.2) can be computed using very efficient algorithms named fast Fourier transform (FFT) [42]. In this study FFT algorithm is used to find frequency spectrum of acoustic signals. It should be noted that the number of FFT points is chosen as power of two nearer to the length of AE events. For those AE events that have fewer points the zero-padding is used before applying DFT, which results in a frequency interpolation.

4.2.2 Acoustic emission entropy using Wavelet transform

The wavelet transform was introduced in the early 1980s [43] and has been used as a useful tool for analyzing transient signals [44].

The continuous wavelet transform (CWT) of a signal f(t) is defined as follows:

$$C(a,b) = \frac{1}{\sqrt{a}} \int f(t)\psi^* \left(\frac{t-b}{a}\right) dt \qquad (4.4)$$

Where $\psi(t)$ is the mother wavelet, a refers to the scale parameter (frequency) and b represents the shifting parameter (time).

By defining the scale parameter a as 2^{-j} and the shifting parameter equal to $k2^{-j}$ the discrete wavelet transform can be computed as follows [43]:

$$C_{j,k} = 2^{j/2} \int f(t)\psi^*(2^j t - k)dt \qquad (4.5)$$

where the resolution level j and the sample time k are integers. The number of levels in wavelet transform should be less than the log two of the length of AE events. In some studies for higher resolution frequency analysis, non-integer values are selected for the resolution level j [45]. The wavelet transform can be done using different mother wavelets. In this study because of the similarity with acoustic emission signals, the Daubechies wavelets with 10 vanishing moments are used [16].

Using the wavelet coefficients (4.5) the energy of the signal in each resolution level can be defined as follows:

$$E_j = \sum_k |C_{j,k}|^2 \qquad (4.6)$$

By defining the total energy as $E_t = \sum_j \sum_k |C_{j,k}|^2$ the probability function can be represented as the relative wavelet energy [30]:

$$Pr_j = \frac{E_j}{E_t} \qquad (4.7)$$

Therefore, by substituting (4.6) in the Shannon entropy (4.1) the wavelet entropy can be defined.

4. 3. Chebyshev's inequality

Assume X is a random variable with expected value μ and variance σ^2. The Chebyshev's inequality proposed for the first time in [46] can be defined for X as follows:

$$\Pr(|x - \mu| \geq k\sigma) \leq \frac{1}{k^2} \qquad (4.8)$$

where k>1 is integer. In other words, for any probability distribution at least $1 - \frac{1}{k^2}$ of the distribution`s values are within k standard deviation of the mean. Based on (4.1) appearing more than $\frac{1}{k^2}$ percent of samples outside the k standard deviation of the mean, means more than one distribution exists.

There are different extensions for the Chebyshev's inequality. The one-sided version of Chebyshev's inequality can be stated by the (4.2):

$$\Pr(x - \mu \geq k\sigma) \leq \frac{1}{1 + k^2} \qquad (4.9)$$

This version has been recognized as Cantelli's inequality that is a generalized Chebyshev's inequality for one tail of the distribution [47].

In this study the one-sided Chebyshev's inequality will be applied to the entropy distribution of acoustic emission signals detected during the FRP tensile test to determine when the maximum recommended load of FRP rods is exceeded. The parameters μ and σ of the entropy histogram are estimated using the detected AE event generated by applying up to the 10-15 percent of the ultimate load to FRP rods. This experiment shows that up to this load the entropies have almost a normal distribution except a few of them that can be considered as outliers for normal distribution. Applying higher level of tensile load to the FRP rods induces progressively higher levels of damage. When there are a small number of damage mechanisms in FRP rods the frequency spectrum of AE events is concentrated in a few frequencies corresponding to the type of damage [14]. Therefore, the AE events with low

entropy are detected that make the left tail of distribution more pronounced. When more damage mechanisms are present in each event in the FRP rods, the frequency spectrum of detected AE events contains broader frequency content causing the entropy of each AE event to increase. This increase in the number of high entropy AE events provides a new distribution in the right tail of AE entropy histogram. Using one-sided Chebyshev's inequality generated by the initial AE events (before 10-15 percent of ultimate load) the existence of new distribution in the right tail can be detected and is used to provide warning when the maximum recommended load of FRP rods is exceeded. One issue concern with using Chebyshev's inequality is finding the mean and standard deviation. Since FRP rods can be damaged in the early stages of loading, the entropy of AE events sourced from these damages can affect the calculation of mean and standard deviation. A robust estimation of μ and σ can be done using the median and median absolute deviation (MAD) [48]. For a data set $x_1, x_2, \dots, x_N$ the MAD is computed as follows:

$$\mathrm{MAD} = \mathrm{median}_i\left(\left|x_i - \mathrm{median}_j(x_j)\right|\right) \qquad (4.10)$$

The mean of data set can be estimated as median and by assuming normal distribution for the data set the standard deviation is estimated as follows [49]:

$$\sigma \approx 1.4826 \times \mathrm{MAD} \qquad (4.11)$$

4.4. Failure prediction using acoustic emission entropy

A series of tensile tests were carried out on FRP rods subjected to ramping load. Matching the maximum frequency range of AE sensor a sampling frequency of 400 kHz was selected for the data acquisition system. A threshold value equivalent to ten times of the noise level was used where, just those AE events that crossed this threshold were detected. The acoustic emission entropy for each detected event was defined by applying a 2048-points discrete

Fourier transform (DFT) and a wavelet transform with a scale parameter varying from 1 to 16 by 0.1 step. Figs. 4.2, 4.3, 4.4, and 4.5 represent the histogram of Fourier transform entropy and Wavelet transform entropy at different percent of ultimate load respectively. The histogram of AE entropy at 10-15 percent of ultimate load was used for extracting the parameters of Chebyshev's inequality. The middle vertical line in each histogram is the mean μ of the histogram that was determined at 10-15 percent of ultimate load and the region restricted to the left and right vertical lines of the mean is within two standard deviation of the mean. These figures show that at the early stages of the load the histogram of the entropy has a shape similar to the normal distribution. Applying more loads to the FRP rods makes the left tail of distribution longer that is related to the smaller entropies. These small entropies mean the frequency spectrum of detected AE event has a few frequency ranges and can be due to a special type of damage that is dominant at the beginning of the test. When the other types of damage increase substantially, the frequency spectrum of AE events contains more frequency bands each one related to a special type of damage [14]. These frequency bands in the spectrum increase the AE entropy. When significant numbers of AE events with high entropy are present, the right tail of AE entropy histogram is longer and a new distribution of high AE entropy events is formed in the right tail. It can be seen that since both left and right tails of the entropy distribution are increased, the average entropy may not be a reliable indicator of increasing damage. However, the right tail that is due to the extreme damage events in FRP rods can be used to determine when maximum recommended load is exceeded. The one-sided Chebyshev's inequality is applied to detect this new distribution in the right tail. According to the one-sided Chebyshev's inequality and by selecting k=2 those AE events that have entropy more than two standard deviation from the mean are considered as the high entropy AE events.

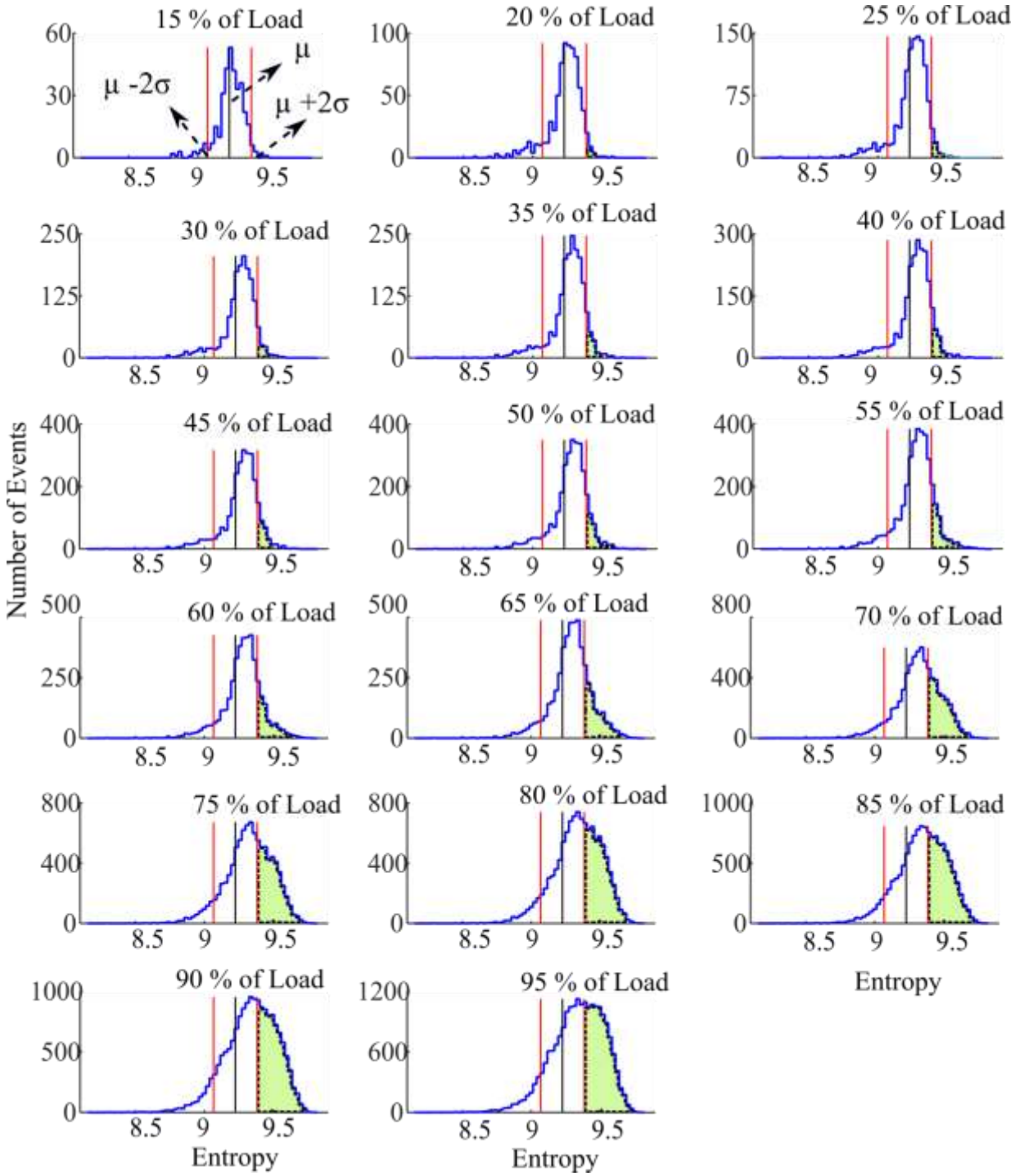

Figure 4. 2 Histogram of the entropy using Fourier transform at different percent of ultimate load for CFRP rod size 2 (The shaded region relates to the high entropy region, the middle black line is the mean of histogram in 15% of ultimate load and the region restricted to the two red lines is within two times of standard deviation from the mean)

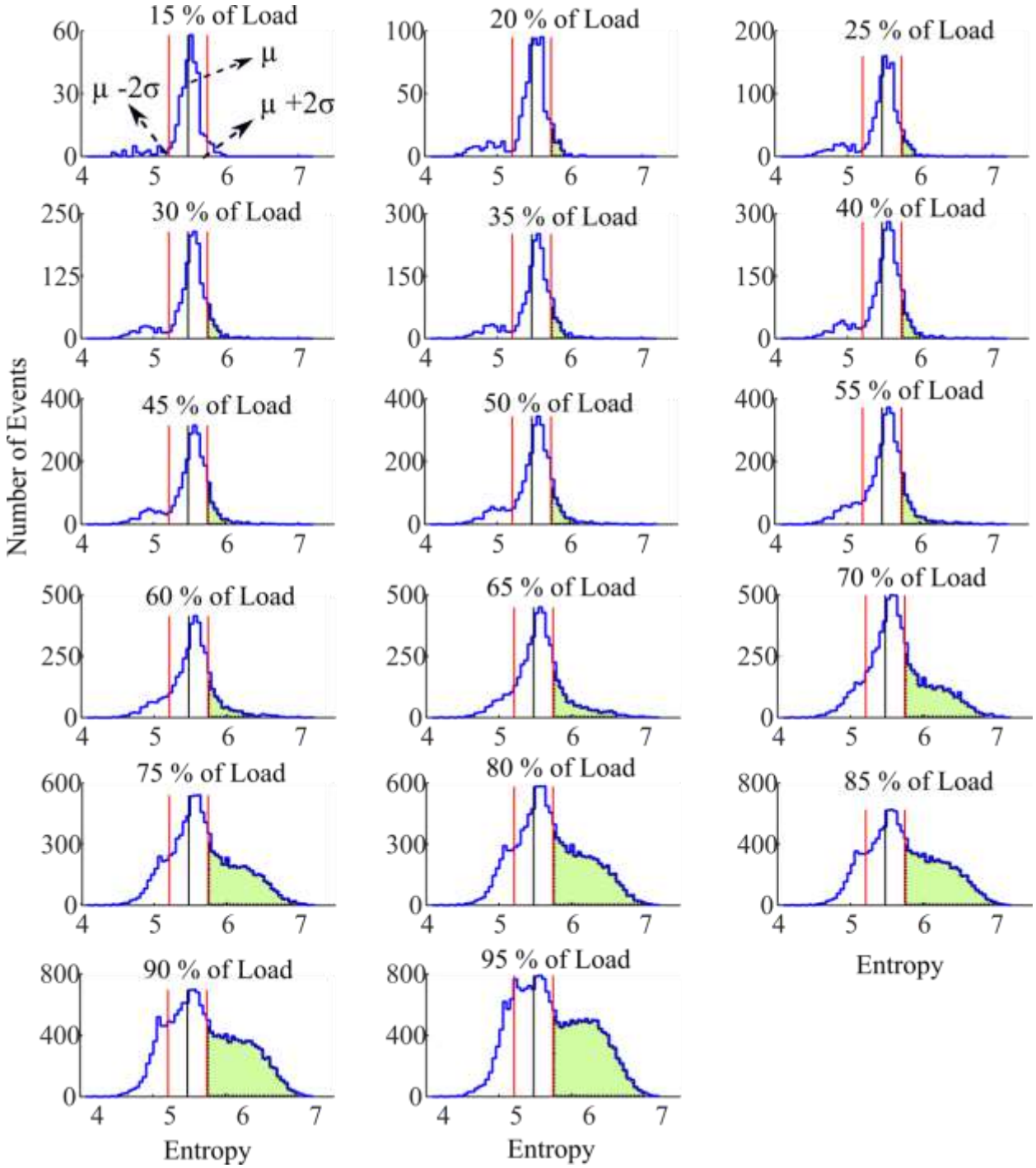

Figure 4. 3 Histogram of the entropy using wavelet transform at different percent of ultimate load for CFRP rod size 2 (The shaded region relates to the high entropy region, the middle black line is the mean of histogram in 15% of ultimate load and the region restricted to the two red lines is within two times of standard deviation from the mean)

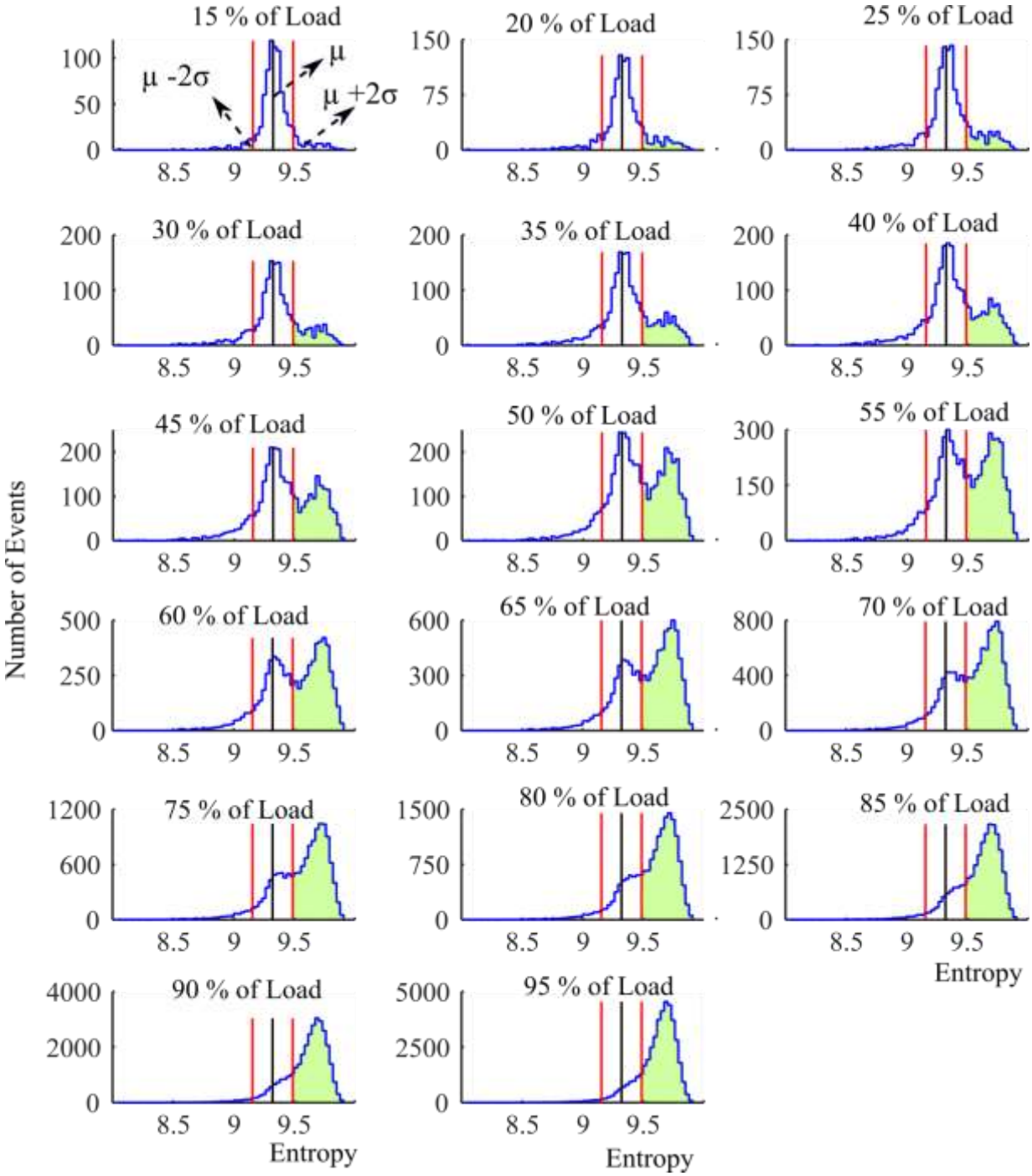

Figure 4. 4 Histogram of the entropy using Fourier transform at different percent of ultimate load for GFRP rod size 6 (The shaded region relates to the high entropy region, the middle black line is the mean of histogram in 15% of ultimate load and the region restricted to the two red lines is within two times of standard deviation from the mean)

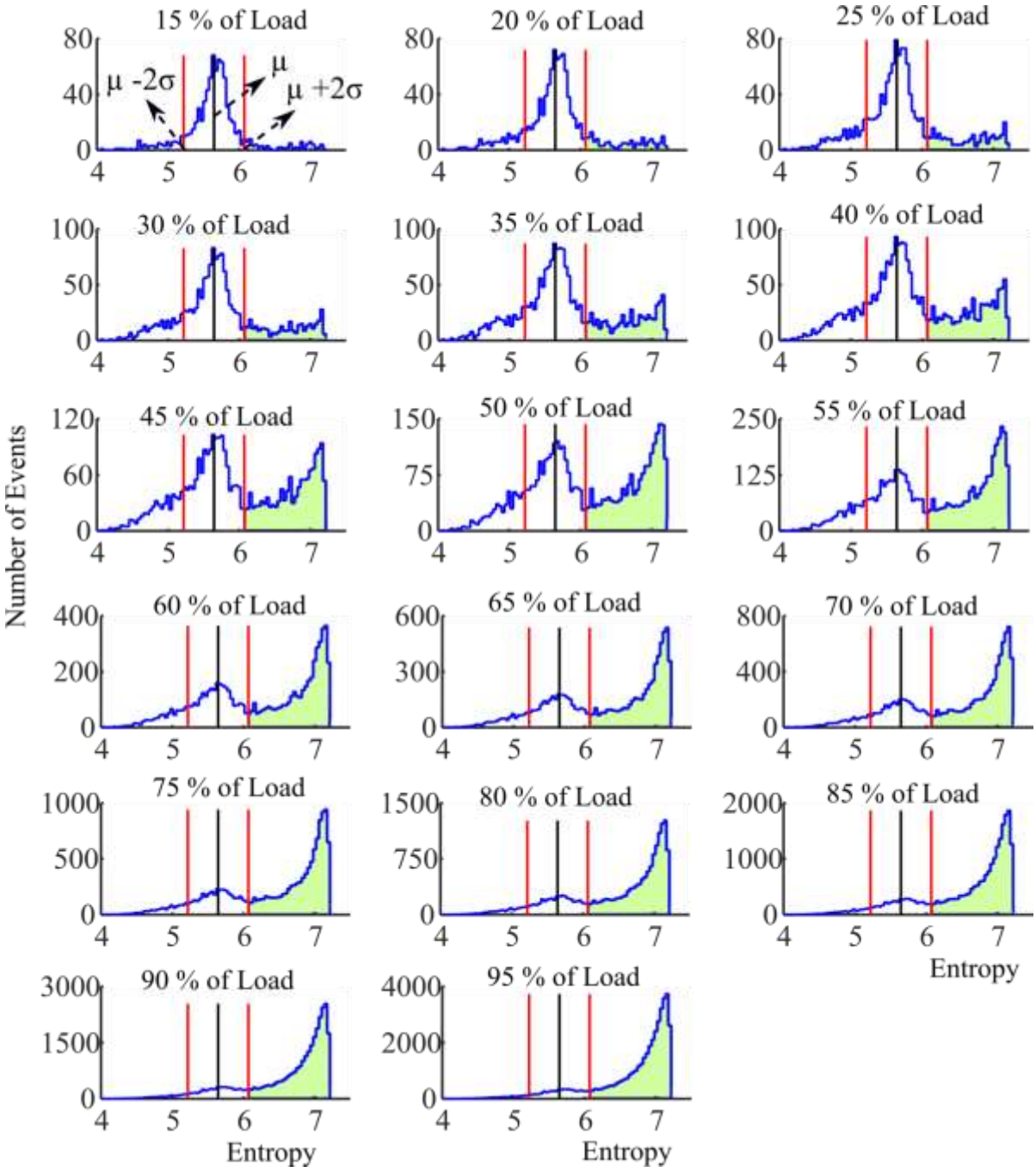

Figure 4. 5 Histogram of the entropy using wavelet transform at different percent of ultimate load for GFRP rod size 6 (The shaded region relates to the high entropy region, the middle black line is the mean of histogram in 15% of ultimate load and the region restricted to the two red lines is within two times of standard deviation from the mean)

Whenever the number of these high entropy AE events passes the $\frac{1}{1+k^2}$ (20% for k=2) a new distribution in the right tail is assumed to have emerged. As it was mentioned this new distribution of high entropy AE events is a result of appearing noticeably different damage mechanisms in FRP rod. Therefore, detecting this new distribution of high AE entropy events can be correlated with the prediction of when the maximum recommended load of FRP rods is exceeded. Figure 4.6 exhibits an example for the percent of amount of high entropy AE events detected using Chebyshev's inequality with k=2 for Fourier transform entropy versus different percent of ultimate load. From this figures it can be seen that for example for GFRP size 4 based on the FFT entropy the evolution curve of high entropy AE events surpasses the Chebyshev's threshold around 42% of ultimate load. Similarly, Chebyshev's criteria can be applied to WT entropy. It means high entropy AE events within the FRP bars, that are the result of simultaneous independent damage mechanisms in the spectrum of AE events, make a new distribution at this point. In this study the entropy technique was used based on the entropy histograms of the accumulated AE events which start from the initial levels of load until ultimate load. The mean and standard deviation values were calculated based on the histograms at 10-15 % of load (baseline data). The histograms at fig. 4.5 and 4.6 represent two distinct distributions which the left distribution was used for determining mean and standard deviation values. It suggests that the mean and standard deviation values can be determined using the histograms at other loads without the baseline data and by distinguishing the two distinct distributions. In Appendix B another method is mentioned to estimate these values without having the baseline data.

Table 4.1 lists the results of exceeding the Chebyshev's threshold for all the FRP bars specimens. From this table it can be seen that the Chebyshev's threshold is exceeded when

GFRP bars exceed averagely 37% of the ultimate load and when CFRP bars exceed averagely 52.4% of the ultimate load.

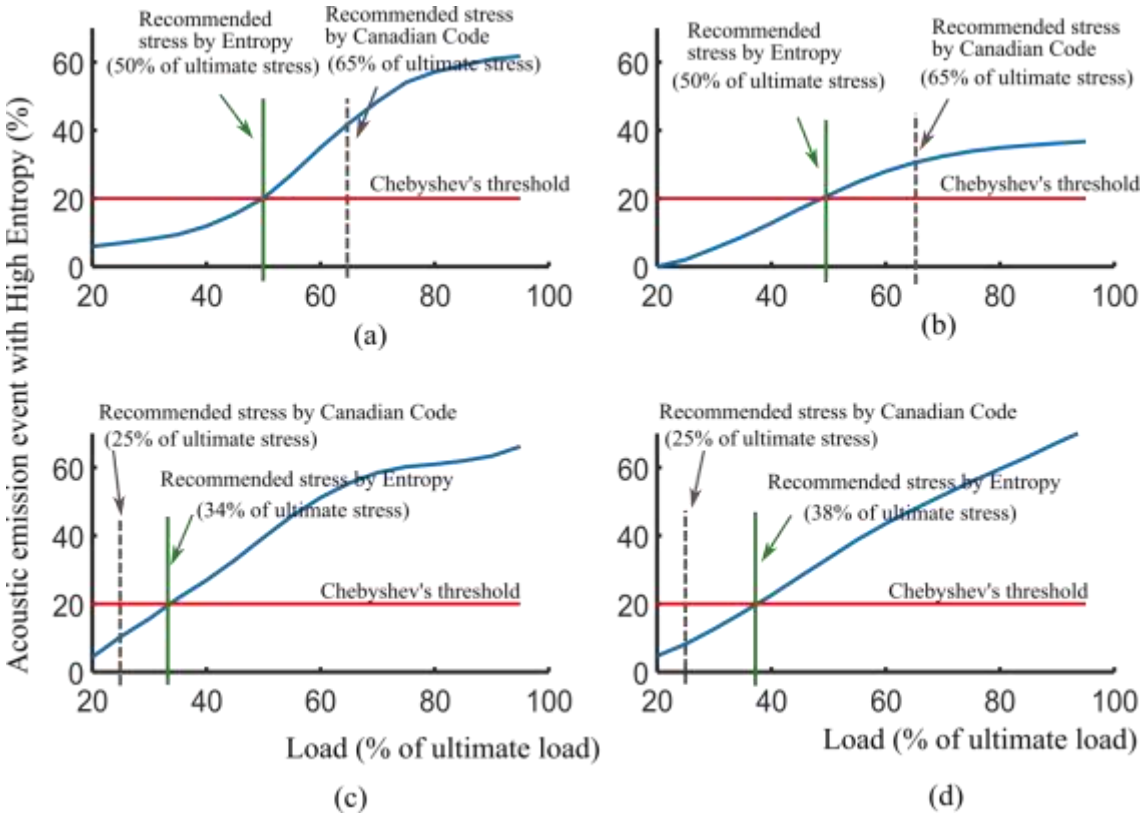

Figure 4. 6 Evolution of the number of AE events with high entropy using Fourier transform in different percent of ultimate load (a) CFRP size 2 (b) CFRP size 4 (c) GFRP size4 (d) GFRP size 6 (The vertical dash line and the vertical solid line refer to recommended stress by Canadian code and recommended stress by entropy method, respectively)

These results demonstrate that monitoring high entropy AE events may provide a useful indicator of when the recommended load of the FRP bars has been reached or exceeded. In other words, when the recommended load is exceeded, the number of high entropy AE events surpasses the Chebyshev's threshold indicating the emergence of a new distribution of high entropy AE events.

Table 4. 1 list of the results of exceeding the Chebyshev's threshold for all the FRP bar specimens

FRP bar type		Chebyshev's threshold crossing (Percent of ultimate load)	
		FFT entropy	WT entropy
CFRP size 2	Specimen 1	~ 65%	~ 65%
	Specimen 2	~ 45%	~ 45%
	Specimen 3	~ 50%	~ 50%
	Average	**~ 53.33%**	**~ 53.33%**
		~ 53.33%	
CFRP size 4	Specimen 1	~ 57%	~ 48%
	Specimen 2	~ 50%	~ 49%
	Average	**~ 53.5%**	**~ 48.5%**
		~ 51%	
GFRP size 4	Specimen 1	~ 34%	~ 32%
	Specimen 2	~ 37%	~ 35%
	Average	**~ 35.5%**	**~ 33.5%**
		~ 34.5%	
GFRP size 6	Specimen 1	~ 42%	~ 32%
	Specimen 2	~ 38%	~ 36%
	Average	**~ 40%**	**~ 34%**
		~ 37%	

Therefore, this algorithm has application in monitoring FRP bars to ensure that safe operating levels have not been exceeded. Moreover, this method may be used for evaluating new FRP systems.

CHAPTER 5: CONCLUSION

Fiber reinforced polymer (FRP) rods have been used for reinforcing in civil structures including concrete structures and steel structures. High strength-to-weight ratio and high resistance to the corrosion make the FRP rods a good replacement for the steel reinforcing rods. The FRP rods become damaged due to excessive loading or accidental sources of damage. Damages in FRP rods degrade the service life of the FRP rods and lead to sudden brittle failure. According to the CAN/CSA-S806-12 standard, the maximum recommended stress in FRP bars under service loads should not exceed 25% and 65% of the ultimate strength for glass FRP (GFRP) and carbon FRP (CFRP), respectively. ACI440.1R recommends that these limits be 20% and 55% for GFRP and CFRP, respectively. These stress values are set to prevent creep failure in FRP bars. However, for in-service applications there are few physical indicators that these values have been reached or exceeded. One of the main drawbacks of the FRP rods compared to the steel reinforcing rods is the lack of ductility. In other words, the stress-strain relationship of these rods is linear and provides no information about failure. Therefore, it is a matter of great importance to develop a technique for determining when the maximum recommended load of FRP rods has been exceeded.

Studies have revealed that acoustic emission (AE) signal analysis is a promising non-destructive damage monitoring technique for FRP materials. When damage such as fibre breakage, matrix cracking and fiber-matrix debonding occurs in FRP rods there is often a sudden release of mechanical energy that results in acoustic emission signals. These acoustic emission signals have been used for damage characterization. This study focussed on providing signal processing approaches based on acoustic emission signals to predict the

incoming failure in FRP rods. To summarize the findings, the following comments can be made:

a) A new methodology named RMS AE event detection compared with the traditional threshold-based method was introduced in Chapter 3 and used to detect AE events separately. The RMS method by using the information in the envelope of the AE signal, overcomes the common problems in the threshold based method. A study of 4180 randomly selected AE events detected by these two methods showed 7.5% error in the RMS method versus 14.7% error in the threshold based method.

b) A fuzzy c-means (FCM) clustering algorithm based on time-based features of the detected AE events in FRP rods was used in Chapter 4 for failure prediction. The scanning electron microscopy (SEM) images admitted the number of clusters. The main hypothesis in this study was that each cluster represents a damage mechanism. The number of events in each cluster was monitored versus the percent of ultimate load. The ratio of the number of AE events in the third FCM cluster to the number of AE events in the first FCM cluster was useful for predicting the failure of the FRP rods. The results of applying this method to four FRP rods showed a significant slope change (factor of 20) in this ratio around 40% and 60% of ultimate load for glass FRP (GFRP) rods and carbon FRP (CFRP) rods, respectively.

c) Frequency spectrum of the detected AE events in FRP rods was used in Chapter 4 for failure prediction. For each AE event the frequency spectrum was found using the FT and WT and then the Shannon entropy was used to measure the randomness of AE events in frequency. It was expected that different damage mechanisms in FRP rods made the frequency spectrum of AE events contain different frequency bands. In other words, more damage mechanisms made the AE spectrum more random. The

results of testing nine different FRP rods showed that at the early stages of the load the AE entropy had a normal distribution. Gradually applying more loads to the FRP rods generated AE events with higher entropies. At higher loads the right tail of AE entropy histogram became longer due to a new distribution of high entropy AE events. The one-sided Chebyshev's inequality generated with the histogram of AE entropy up to 10-15% of ultimate load was applied to detect this new distribution in the right tail. According to the one-sided Chebyshev's inequality with k=2 those AE events that had entropy more than two standard deviation from the mean were considered as the high entropy AE events. Whenever the number of these high entropy AE events passed the $\frac{1}{1+k^2}$ (20% for k=2) the new distribution in the right tail was detected. Detection of this new distribution of high AE entropy events was correlated with the determination of when maximum recommended load of FRP rods is exceeded. The diagram of percent of AE event with high entropy versus different percent of ultimate load represented that this distribution occurred averagely at 37% and 52.4% ultimate load for GFRP and CFRP, respectively.

d) Both the pattern recognition technique and frequency entropy method, showed comparable results with the standard CAN/CSA-S6-06, and CAN/CSA-S806-02, where the maximum permissible stresses in GFRP and CFRP tendons are 25% and 65% of the ultimate load.

5.1 Recommendation for future research

a) Corrosion is the major cause of civil engineering installations degradation. Acoustic emission signal processing has been used excessively in corrosion detection. The RMS AE event detection technique combined with the frequency entropy method

described in Chapter 4 is strongly recommended to be used for corrosion detection, since corrosion can expand the frequency spectrum of AE events.

b) The RMS technique combined with the frequency entropy technique can be implemented on a microcontroller and be used as for online monitoring of FRP rods installations.

REFERENCES

[1] Teng JG, Yu T, Fernando D. Strengthening of steel structures with fiber-reinforced polymer composites. Journal of Constructional Steel Research. 2012 Nov 30;78:131-43.

[2] You YJ, Park YH, Kim HY, Park JS. Hybrid effect on tensile properties of FRP rods with various material compositions. Composite structures. 2007 Sep 30;80(1):117-22.

[3] Suratno, Basuki R., Lin Ye, and Yiu-Wing Mai. "Simulation of temperature and curing profiles in pultruded composite rods." *Composites Science and Technology* 58.2 (1998): 191-197.

[4] J.P. Busel, Fiber reinforced polymer (FRP) composites rebar, American Composites Manufacturers Association (2012).

[5] Intelligent Sensing for Innovative Structures (ISIS) Canada, Reinforcing Concrete Structures with Fibre Reinforced Polymers, ISIS Canada Research Network, Design Manual No. 3, Version 2 (2007)

[6] Mufti AA, Onofrei M, Benmokrane B, Boulfiza M, Newhook JP, Bakht B, Tadros G, Brett P. Report on the studies of GFRP durability in concrete from field demonstration structures. In Proceedings of the Conference on Composites in Construction 2005 Jul (pp. 11-13).

[7] Kumar CS, Arumugam V, Sajith S, Dhakal HN, John R. Acoustic Emission Characterisation of Failure Modes in Hemp/Epoxy and Glass/Epoxy Composite Laminates. Journal of Non-destructive Evaluation. 2015;34(4):1-1.

[8] S. Barre´, M.L. Benzeggagh, On the use of acoustic emission to investigate damage mechanisms in glass-fibre-reinforced polypropylene, Composites Science and Technology 52(1994) 369–76.

[9] Berthelot J-M, Rhazi J. Acoustic emission in carbon fiber composites. Composites Science and Technology 1990;37:411–28.

[10] Tsamtsakis D, Wevers M, Demesster P. 1998 Acoustic emission from CFRP laminates during fatigue loading. Journal of reinforced plastics and composites 1998;17:1185-1201.

[11] A.M. Calabrò, C. Esposito, A. Lizza, M. Giordano, A. D'amore, L. Nicolais, Analysis of the acoustic emission signals associated to failure modes in CFRP laminates, ECCM 8 Conference Proceedings, Naples 8(1998) 425-432.

[12] D. Valentin, P. Bonniau, A. Bunsell, Failure mechanism discrimination in carbon fiber-reinforced epoxy composites, Composites 14.4(1983) 345-351.

[13] Komai K, Minoshima K, Shibutani T. Investigations of the fracture mechanism of carbon/epoxy composites by AE signal analyses. JSME international journal. Ser. 1, Solid mechanics, strength of materials. 1991 Jul 15;34(3):381-8.

[14] Gutkin R, Green C, Vangrattanachai S, Pinho S, Robinson P, Curtis P. On acoustic emission for failure investigation in CFRP: Pattern recognition and peak frequency analyses. Mechanical Systems and Signal Processing 2011;25:1393-1407.

[15] Godin N, Huguet S, Gaertner R, Salmon L. Clustering of the acoustic emission signals collected during tensile tests on unidirectional glass/polyester composite using supervised and unsupervised classifiers. NDT&E International 2004;37:253-264.

[16] Marec A, Thomas J, El Guerjouma R. Damage characterization of polymer-based composite materials: Multivariable analysis and wavelet transform for clustering acoustic emission data. Mechanical Systems and Signal Processing 2008;22:1441–1464.

[17] Q. Ni, M. Iwamoto, Wavelet transform of acoustic emission signals in failure of model composites, Engineering Fracture Mechanics 69(2002) 717-728.

[18] P.J. De Groot, P.A. Wijnen, R.B. Janssen. Real-time frequency determination of acoustic emission for different fracture mechanisms in carbon/epoxy composites, Composites Science and Technology 55.4(1995) 405-12.

[19] C.R. Ramirez-Jimenez, N. Papadakis, N. Reynolds, T.H. Gan, P. Purnell, M. Pharaoh, Identification of failure modes in glass/polypropylene composites by means of the primary frequency content of the acoustic emission event, Composites Science and Technology 64.12(2004) 1819-27.

[20] A. Bussiba, M. Kupiec, R. Piat, T. Böhlke, Fracture characterization of C/C composites under various stress modes by monitoring both mechanical and acoustic responses, Carbon 46.4(2008) 618-30.

[21] G. Qi, Wavelet-based AE characterization of composite materials, NDT & E International, 33.3(2000) 133-44.

[22] T.H. Loutas, V. Kostopoulos, C. Ramirez-Jimenez, M. Pharaoh, Damage evolution in center-holed glass/polyester composites under quasi-static loading using time/frequency analysis of acoustic emission monitored waveforms, Composites science and technology 66.10(2006) 1366-75.

[23] R. Unnthorsson, T. Runarsson, M. Jonsson, AE entropy for the condition monitoring of CFRP subjected to cyclic fatigue, Journal of Acoustic Emission 26(2009) 262–269.

[24] Gostautas R-S, Ramirez G, Peterman R-J, Meggers D. Acoustic emission monitoring and analysis of glass fiber reinforced composites bridge decks. Journal of bridge engineering 2005;10(6):713-21.

[25] Y. Liang, C. Sun, F. Ansari, Acoustic emission characterization of damage in hybrid fiber-reinforced polymer rods. Journal of Composites for Construction 2004;8(1):70-8.

[26] Theobald P, Zeqiri B, Avison J. Couplants and their influence on AE sensor sensitivity. J Acoust Emission 2008;26:91–7.

[27] Hsu N, Breckenridge F. Characterization of acoustic emission sensors. Mater. Eval. 1981;39:60-68.

[28] Grabec I, Sachse W. Application of an intelligent signal processing system to acoustic emission analysis. The Journal of the Acoustical Society of America. 1989 Mar 1;85(3):1226-35.

[29] Promboon, Y., 2000, Acoustic Emission Source Location", Dissertation presented for degree of Doctor of Philosophy, The University of Texas at Austin.

[30] Chapra SC, Canale RP. Numerical methods for engineers. New York: McGraw-Hill; 2012.

[31] Wevers M. Listening to the sound of materials: acoustic emission for the analysis of material behaviour. NDT&E International 1997;30(2):99-106

[32] Barsoum F, Suleman J, Korcak A, Hill E. Acoustic emission monitoring and fatigue life prediction in axially loaded notched steel specimens. Journal of Acoustic Emission 2009;27:40-63

[33] Arumugam V, Sajith S, Stanley AJ. Acoustic emission characterization of failure modes in GFRP laminates under mode I delamination. Journal of Nondestructive Evaluation. 2011 Sep 1;30(3):213-9

[34] Unnthorsson R, Runarsson T, Jonsson M. Acoustic emission based fatigue failure criterion for CFRP. International journal of fatigue 2008;30:11-20

[35] Torres-Arredondo MA, Tibaduiza DA, McGugan M, Toftegaard H, Borum KK, Mujica LE, Rodellar J, Fritzen CP. Multivariate data-driven modelling and pattern recognition for damage detection and identification for acoustic emission and acousto-ultrasonics. Smart Materials and Structures. 2013;22(10):105023

[36] Bezdek J, Ehrlich R, Full W. FCM: The fuzzy C-mean clustering algorithm. Computer & Geosciences 1984;10(2-3):191-203.

[37] Rezaee M, Lelieveldt B, Reiber J. A new cluster validity index for the fuzzy C-mean. Pattern recognition letters 1998;19:237-246.

[38] Pal N, Bezdek J. On cluster validity for the fuzzy c-means model. IEEE Trans. Fuzzy Syst. 1995;3:370-379.

[39] Bensaid A, Hall L, Bezdek J, Clarke L, Silbiger M, Arrington J, Murtagh R. Validity-guided (re) clustering with applications to image segmentation. IEEE Trans Fuzzy Syst.1996;4:112–123

[40] Xie, X. L. and Beni, G. [1991]. A validity measure for fuzzy clustering, IEEE Trans Pattern Anal,13, 841–847.

[41] C.E. Shannon, A Mathematical Theory of Communication, The Bell System Technical Journal 27(1948) 27: 379–423, 623–656.

[42] J.G. Proakis, D.G. Manolakis, Digital signal processing 3rd edition, New Jersey: Prentice-Hall 1996.

[43] A. Grossmann, J. Morlet, Decomposition of Hardy functions into square integrable wavelets of constant shape, SIAM journal on mathematical analysis 15.4(1984) 723-36

[44] I. Daubechies, Ten lectures on wavelets, Philadelphia: Society for industrial and applied mathematics 1992.

[45] A. Prochazka, N. Kingsbury, P.J. Payner, J. Uhlir, Signal analysis and prediction, Springer Science & Business Media 2013.

[46] I.J. Bienaymé, Considérations à l'appui de la découverte de Laplace sur la loi de probabilité dans la méthode des moindres carrés, Imprimerie de Mallet-Bachelier 1853.

[47] F.P. Cantelli, Intorno ad un teorema fondamentale della teoria del rischio, Tip. degli operai; 1910.

[48] C. Leys, C. Ley, O. Klein, P. Bernard, L. Licata, Detecting outliers: Do not use standard deviation around the mean, use absolute deviation around the median, Journal of Experimental Social Psychology 49.4(2013) 764-6.

[49] Analytical Methods Committee, Robust statistics: a method of coping with outliers, Technical brief 2001.

APPENDIX A

This appendix contains the proof of equation (3.1) that relates the Ratio parameter in RMS algorithm with M_{thr} and F_{thr}. According to the definition, the Ratio parameter is the maximum acceptable ratio of valley to peak of an AE event. Based on RMS algorithm generally there are two different types of valley that can be seen in fig. A.1.

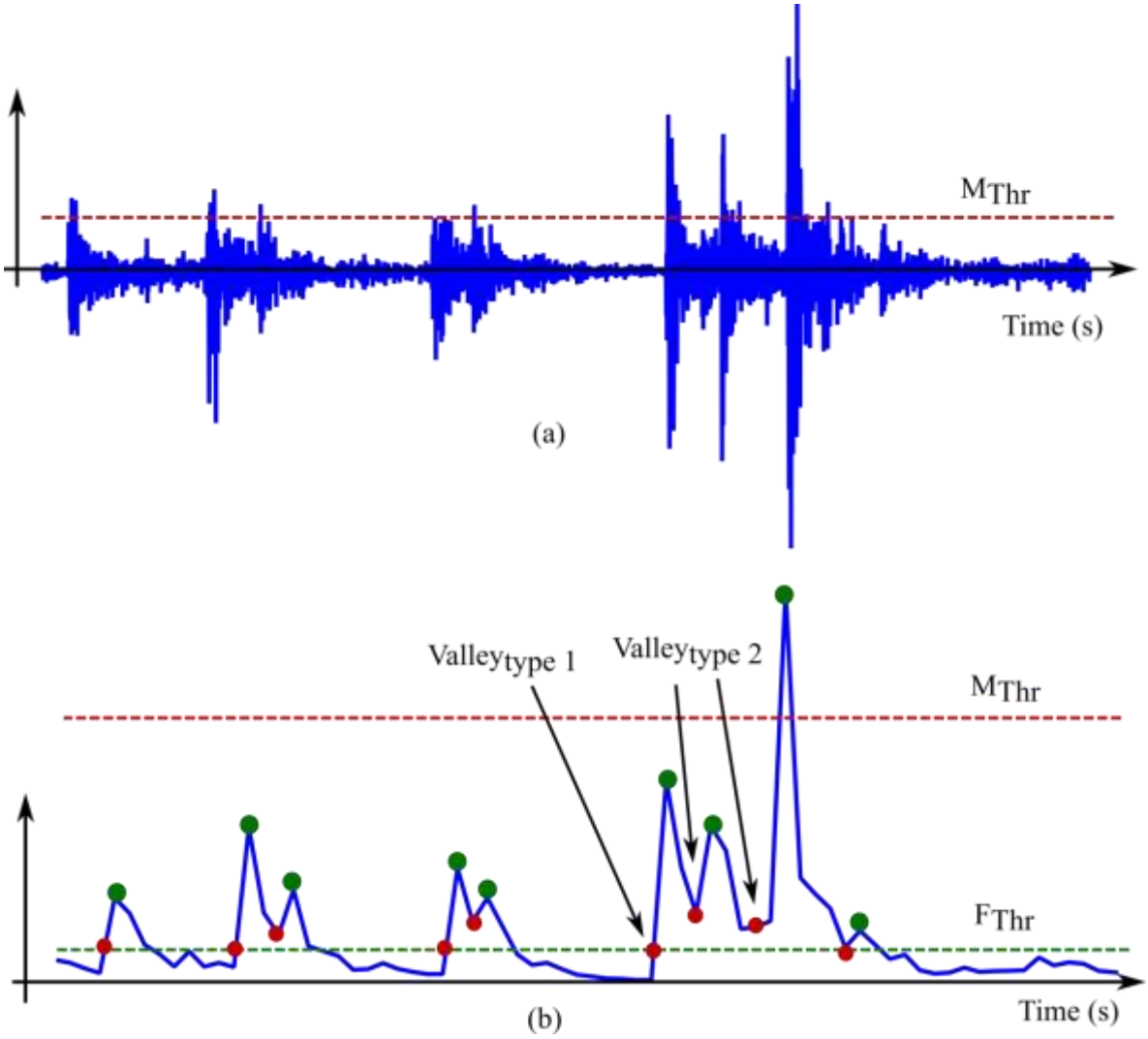

Figure A. 1 Different types of valley in the RMS form of acoustic emission signal (a) Acoustic emission signal (b) RMS form of acoustic emission signal

First type of valley that is related to the beginning of the detected interval is very close to the F_{thr}. For the value of peak, the worst case is when it is less than M_{thr} –that absolutely is more than the F_{thr}–. By assuming that the peaks in this scenario have uniform distribution in interval $[F_{thr}, M_{thr}]$ (means maximum randomness) the value of peak in average is $\frac{F_{thr}+M_{thr}}{2}$. Thus, in this case the Ratio is as follows:

$$\text{Ratio} = \frac{F_{thr}}{\frac{(M_{thr}+F_{thr})}{2}} = \frac{2F_{thr}}{(M_{thr}+F_{thr})} \quad \text{(A.1)}$$

emission signal (b) RMS form of acoustic emission signal

Second type of valley usually appeared at the middle of a detected interval. This type is more than F_{thr} but still is less than the peak. It means the valleys in this scenario are distributed in interval $[F_{thr}, \frac{(M_{thr}+F_{thr})}{2}]$. By assuming uniform distribution for valleys in this scenario, the value of valley averagely is $\frac{F_{thr}+\frac{(M_{thr}+F_{thr})}{2}}{2}$. Therefore, the Ratio is as follow:

$$\text{Ratio} = \frac{\frac{F_{thr}+\frac{(M_{thr}+F_{thr})}{2}}{2}}{\frac{(M_{thr}+F_{thr})}{2}} = \frac{M_{thr}+3F_{thr}}{2(M_{thr}+F_{thr})} \quad \text{(A.2)}$$

By comparing (A.1) with (A.2) it can be found that Ratio parameter in (A.2) is larger. Therefore, the maximum ratio of valley to peak in RMS algorithm is (A.2).

APPENDIX B

This appendix represents how the Entropy method can be used for in-service structures. The entropy technique is based on the Chebyshev's threshold which needs the baseline data to determine the initial entropy distribution and extract mean and standard division values. However, these values can be estimated without having the baseline data. For example, to calculate frequency entropy, 2048-points Fast Fourier transform (FFT) was used. The first 1024 of these coefficients are related to the positive frequencies and are directly used to define probability function as follows:

$$\Pr(\mathrm{X} = \mathrm{X_i}) = \frac{|\mathrm{X_i}|}{\sum_{j=0}^{\frac{N}{2}-1} |\mathrm{X_j}|} \qquad i = 0,1,\dots,\frac{N}{2} - 1 \qquad (B.1)$$

where $|\mathrm{X_i}|$ is the magnitude of signal in the i-th frequency.

This probability function is for the frequency range 0-200 kHz. Based on the frequency range of the AE transducer 80-200 kHz and the sampling frequency 400 kHz in this experiment, about 409 of FFT coefficients are in 0-80 kHz. This range can be associated with the unwanted signal and should have small amplitude and therefore small probability values (See Fig.4.1). The main AE signal should exist in 80-200 kHz. Let's consider

$$\begin{cases} p_{US} = p_1 + p_2 + \cdots + p_n = \alpha \\ p_{MS} = p_{n+1} + \cdots + p_{1024} = 1 - \alpha \end{cases} \qquad 0 < \alpha < 1 \qquad (B.2)$$

Where p_i is the probability function defined for ith coefficient, p_{US} and p_{MS} refer to the probability function of unwanted signal and main signal respectively and n is the number of coefficients related to the unwanted signal. The value of α should be very small since the unwanted signal has smaller amplitude compare to the main signal. As it was mentioned there are 409 coefficients related to unwanted signal in 0-80 kHz and there might be a few

more unwanted coefficients with small amplitude in the 80-200 kHz generated by background noise. By considering the above explanation, the highest entropy can be found by assuming uniform distributions for both unwanted and main signals, i.e.

$$\begin{cases} p_{US}: p_1 = p_2 = \cdots = p_n = \alpha/n \\ p_{MS}: p_{n+1} = \cdots = p_{1024} = \dfrac{1-\alpha}{1024-n} \end{cases} \qquad (B.3)$$

In this case the entropy can be calculated as follows:

$$\mathrm{H(X)} = -\sum_{\mathrm{i=1}}^{1024} \mathrm{Pr(x = x_i)\log 2(Pr(x = x_i))}$$

$$= -\sum_{i=1}^{n} \frac{\alpha}{n} log2(\frac{\alpha}{n}) - \sum_{i=n+1}^{1024} \frac{1-\alpha}{1024-n} log2(\frac{1-\alpha}{1024-n}) \qquad (B.4)$$

Therefore

$$\mathrm{H(X)} = -\alpha log2\left(\frac{\alpha}{n}\right) - (1-\alpha) log2\left(\frac{1-\alpha}{1024-n}\right) \quad (B.5)$$

By considering a range of 409-500 for n and $e < \alpha < 0.01$ where $e \approx 0$ a set of entropies can be calculated based on equation B.5 (see Fig .B.1).

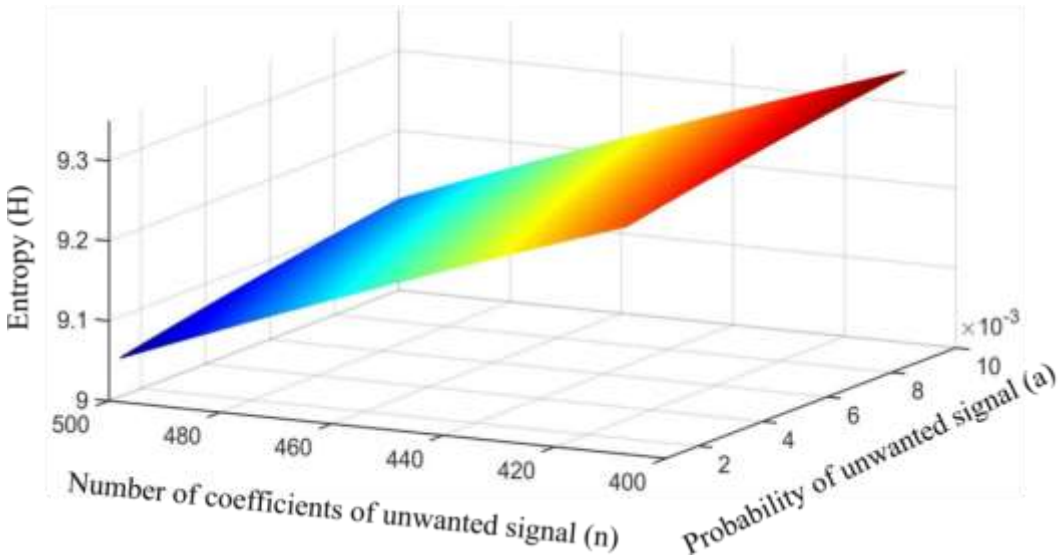

Figure B. 1 Approximation of the entropy based on the equation B.5

The figure B.1 provides entropy values for approximated number of coefficients of unwanted signal and probability of unwanted signal by assuming uniform distributions for both unwanted and main signals. Based on this figure, the mean and standard division values are calculated as 9.20 and 0.085 respectively. For practical data higher values may be found since the sensor doesn't perform ideal in 0-80 kHz and therefore there might exist main signal in this range which makes the entropy increases. Now, we return to the real data and calculate the mean and standard division used by Chebyshev. Table B.1 list these values for each specimen.

Table B. 1 list of the Chebyshev's Parameters for all the FRP rod specimens

FRP rod type		Chebyshev's Parameters FFT entropy	
		μ	σ
CFRP size 2	Specimen 1	9.21	0.086
	Specimen 2	9.22	0.080
	Specimen 3	9.19	0.10
CFRP size 4	Specimen 1	9.26	0.091
	Specimen 2	9.24	0.098
GFRP size 4	Specimen 1	9.21	0.11
	Specimen 2	9.25	0.106
GFRP size 6	Specimen 1	9.27	0.083
	Specimen 2	9.27	0.10

It can be seen that the mean values and standard division values listed in this table are very close to the above approximated values. Therefore, to apply entropy method to the in-service structure although the baseline data are not available for mean and standard division values calculations, the approximated values based on Fig.B.1 can be used.

APPENDIX C

This appendix provides a raw idea based on the accumulated energy of AE signals that might be used for failure prediction. Moreover it suggests three frequency ranges in AE signals which could be associated to different damage mechanisms (more study is needed).

Fig. C.1 shows accumulated energy behavior of different FRP rods. For the CFRP rods the accumulated energy increases gradually until the failure. On the other hand, for the GFRP rods the accumulated energy has a significant rise close to the failure. This energy behaviour of CFRPs will be used for failure prediction in the CFRP rods.

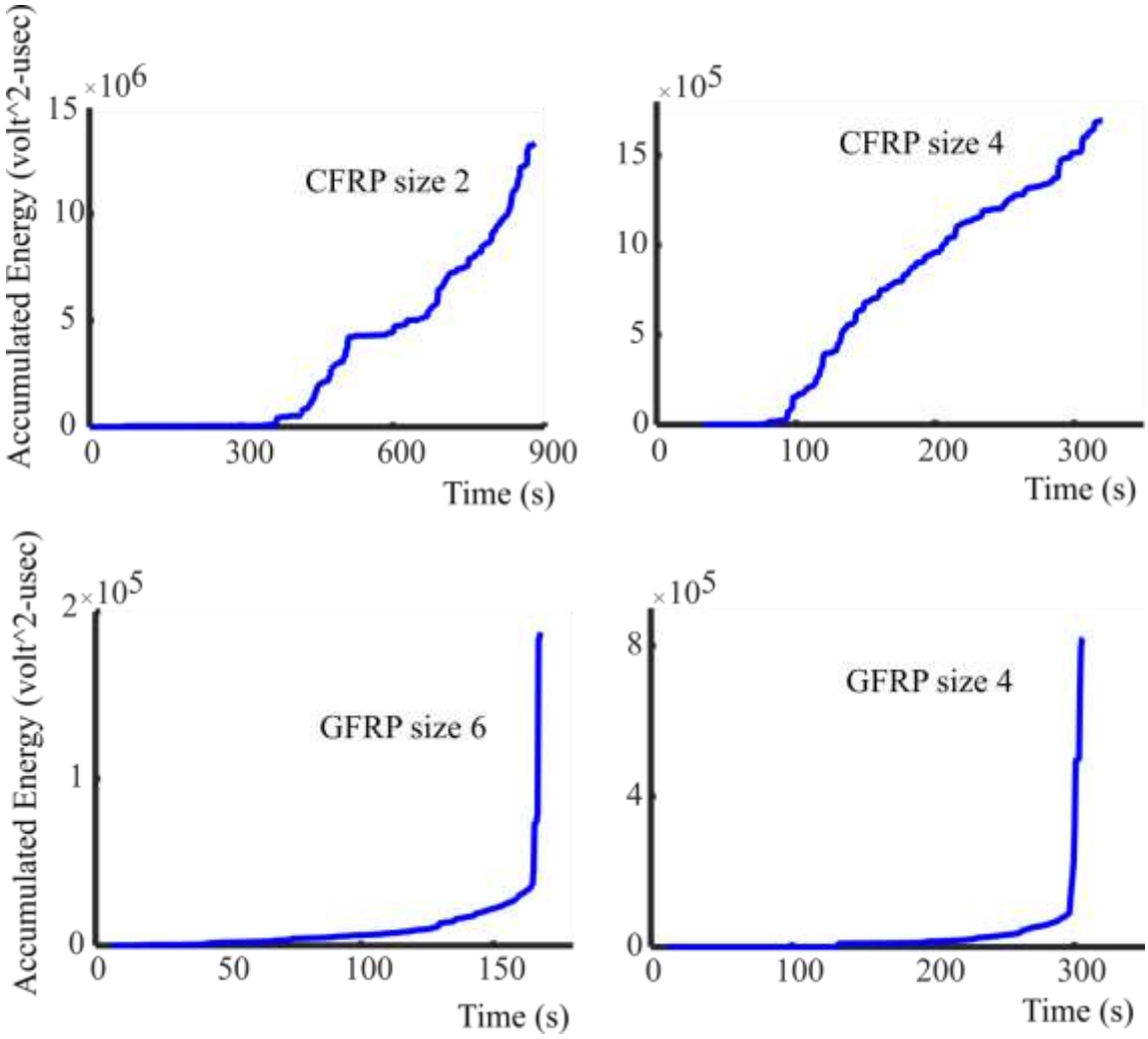

Figure C. 1 Accumulated energy behavior of various types of fiber reinforced polymer rods

As it was stated in Chapter 1 damage mechanisms in composite materials were characterized based on the frequency of AE signals by [14, 18-20]. It was assumed that different damage mechanisms generate specific frequency range. For each acoustic emission event, the peak frequency is defined as the frequency at which the magnitude of the FFT is maximum. Fig. C.2 provides an example of AE signal and associated peak frequency.

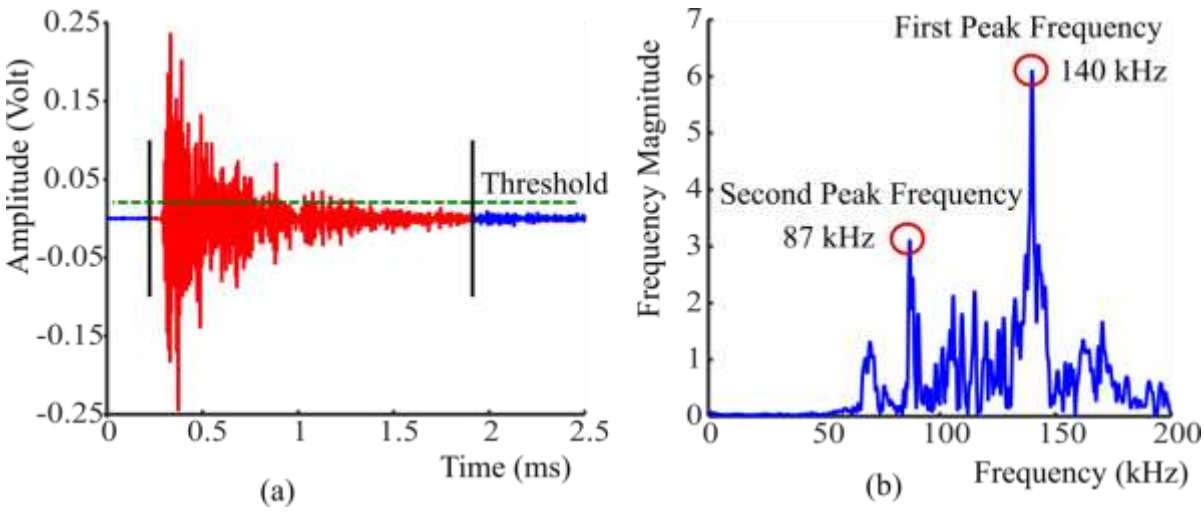

Figure C. 2 (a) Acoustic emission event waveform (b) fast Fourier transform (FFT) of acoustic emission event

Three different cluster validity indexes are used to find optimum number of clusters in the peak frequencies of acoustic emission events. The partition coefficient (PC) and partition index (PI) are used (These indexes were introduced in Chapter 3). As it was stated the PC index measures the amount of overlapping between the clusters. Optimum number of clusters maximizes this index. In practice for the optimum number of cluster, the PC index shouldn't be much lower than 1. The PI index measure the compactness of the clusters and optimum number of clusters should minimize this parameter. Fig. C.3 represents the optimum number of clusters in AE frequencies based on the two mentioned indexes.

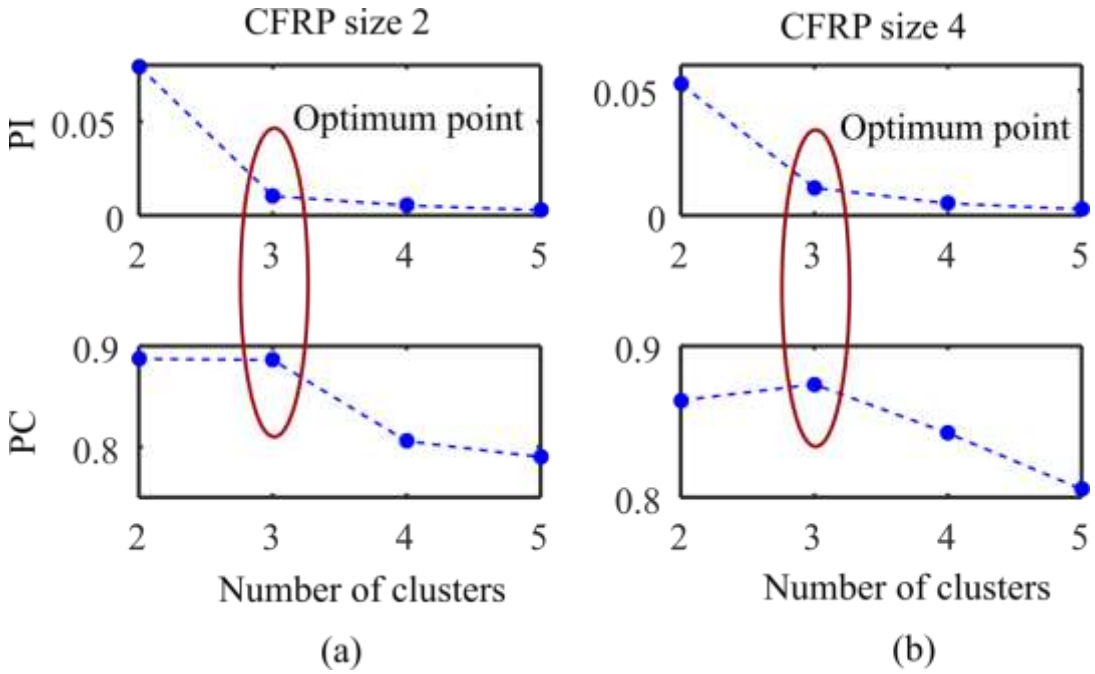

Figure C. 3 Cluster validity results using two different indexes for (a) CFRP size 2 and (b) CFRP size 4

Based on Fig. C.3 three clusters can be considered in peak frequencies of AE signals. Similarly, the scanning electron microscope images in Fi. C.4 shows three main damage mechanisms in tested FRP rods.

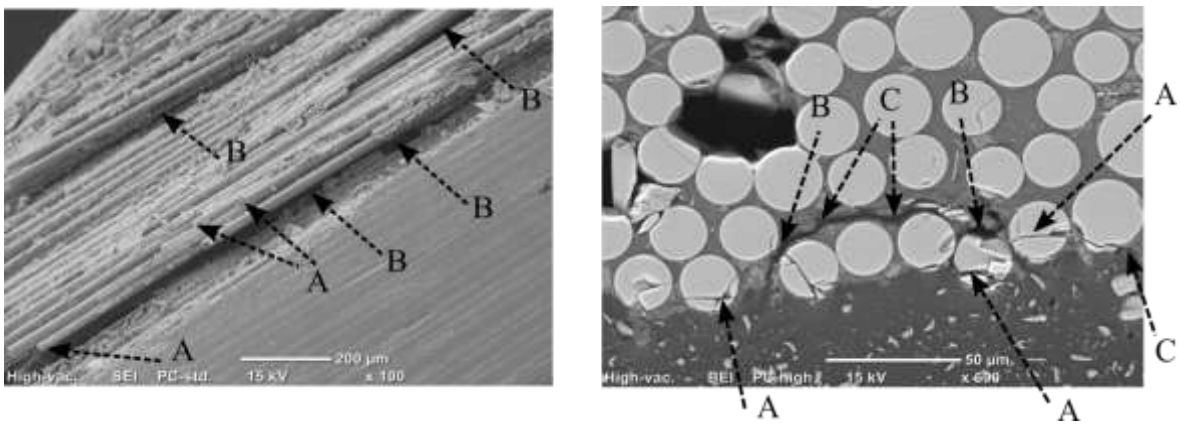

Figure C. 4 Scanning electron microscopy (SEM) image of FRP rod after tensile test, A, B and C refer to the fiber breakage, fiber-matrix debonding and matrix cracking, respectively.

However, more studies are needed to associate each funded clusters to a specific damage mechanism. Based on the mentioned explanation, the Fuzzy c-means clustering algorithm (defined in Chapter 3) with three clusters is used to discriminate the AE events based on the peak frequencies.

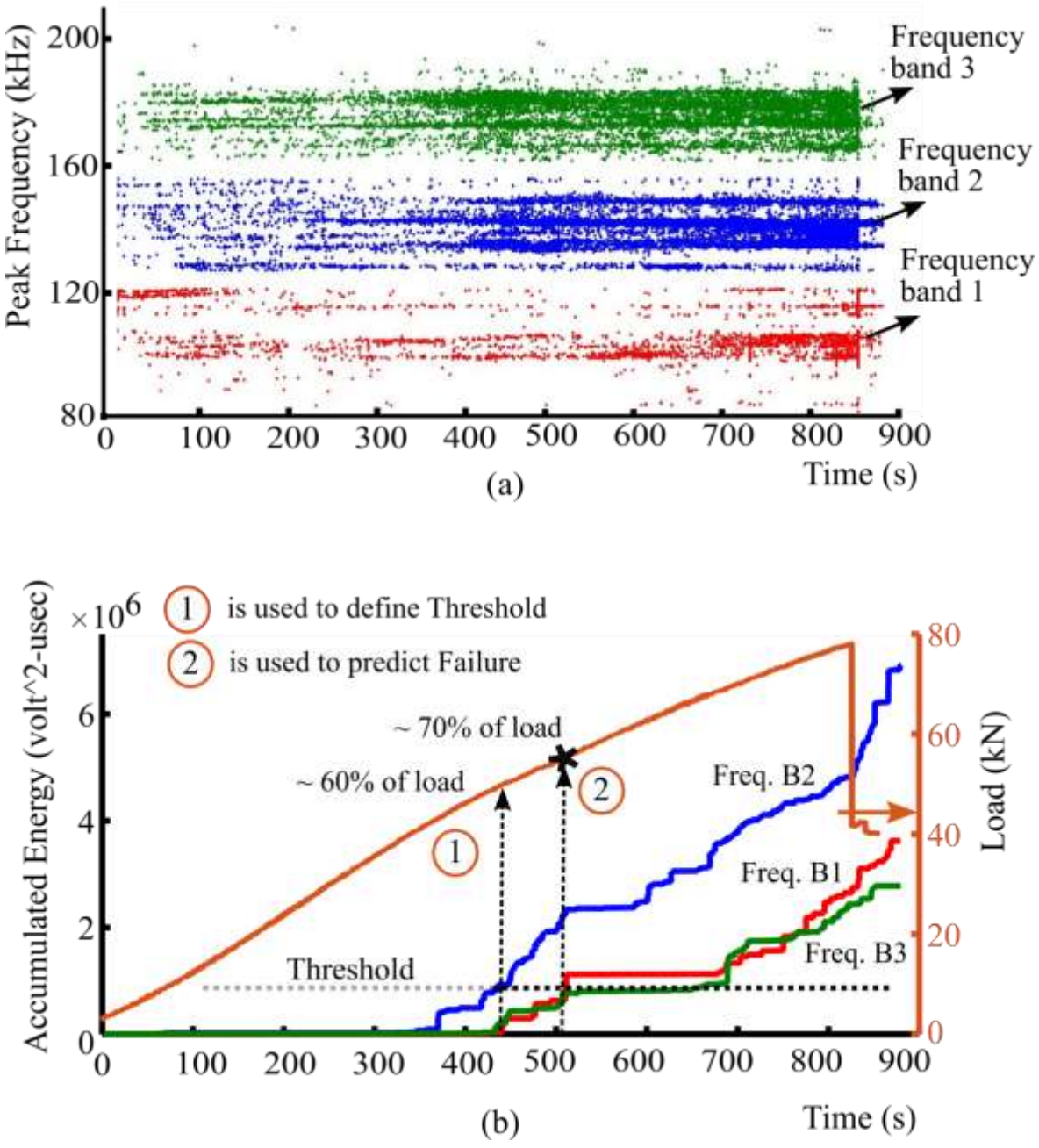

Figure C. 5 (a) Results of fuzzy c-means algorithm with three clusters and (b) accumulated energy behaviour for each cluster for CFRP size 2

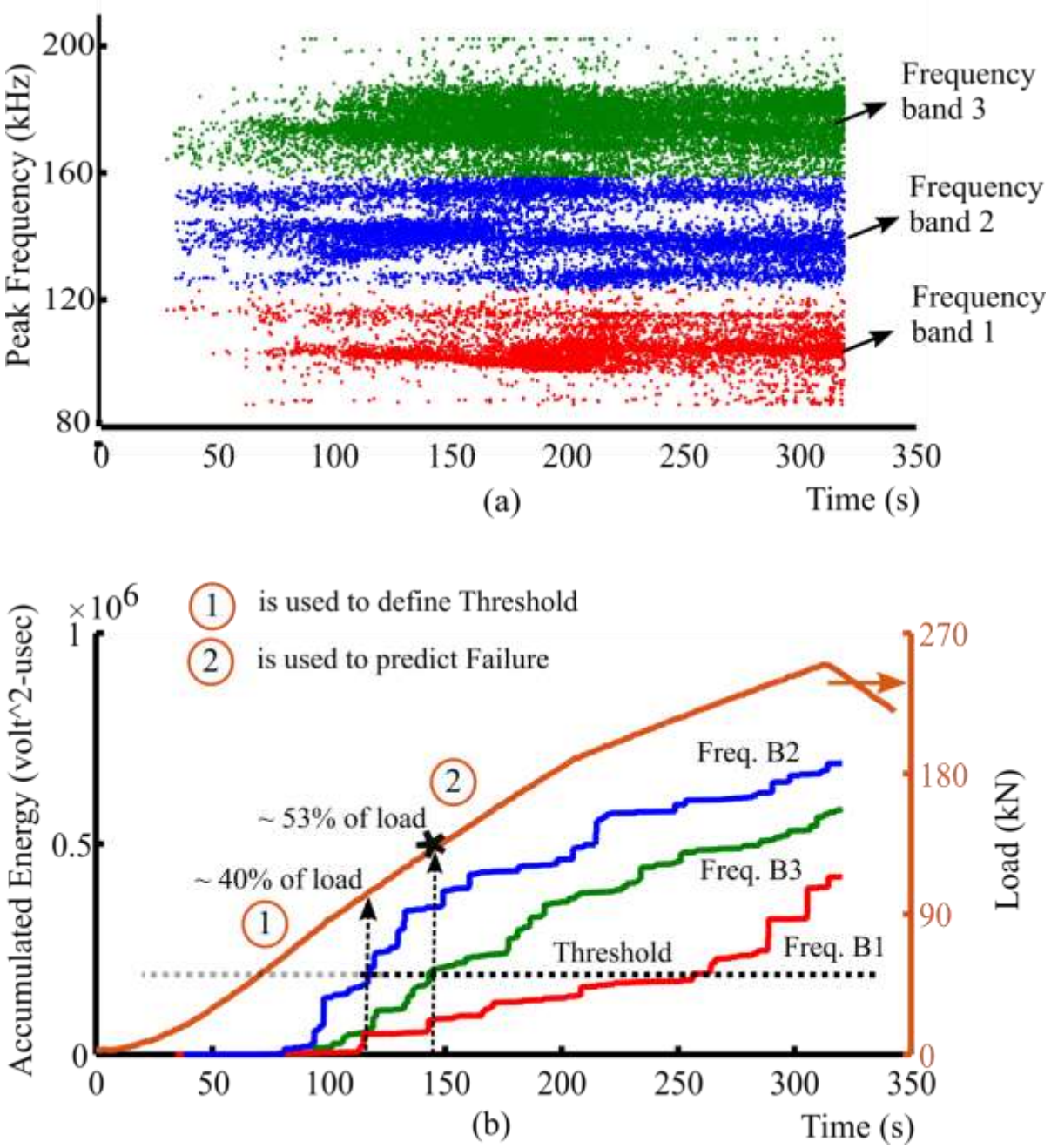

Figure C. 6 . (a) Results of fuzzy c-means algorithm with three clusters and (b) accumulated energy behaviour for each cluster for CFRP size 4

Based on Figs C.5 and C.6 a method for prediction of incoming failure can be suggested. The accumulated energy of the frequency band 2 rises first. The level of energy at which the accumulated energy of the other two clusters rises is defined as the threshold. The threshold crossing is used for the failure prediction. Moreover, based on these figures three frequency

bands are suggested as stated in Fig. C.7. To associate each frequency band to a damage mechanism for FRP rods, more research is suggested as the future work.

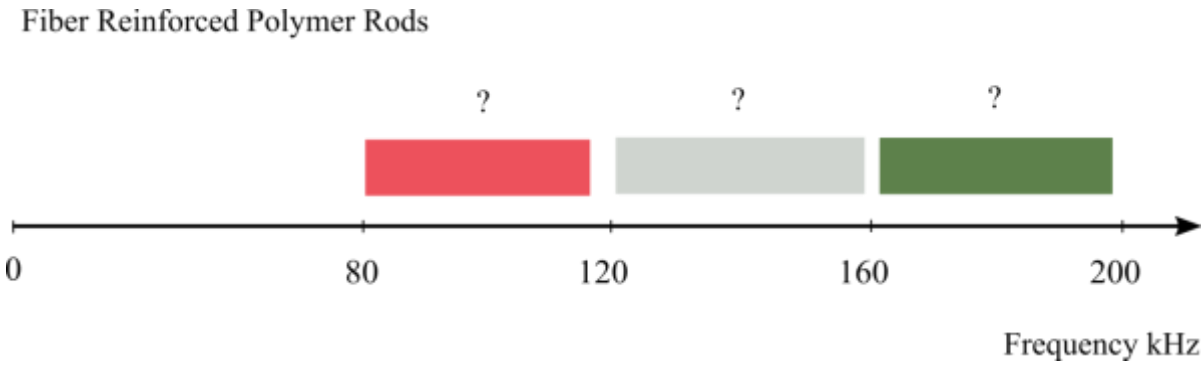

Figure C. 7 Peak frequency ranges of AE signals associated to Carbon Fiber Reinforced Polymer rods.